UNCLASSIFIED

[redacted]

Copy

RM SL50K01

[redacted]

NACA

RESEARCH MEMORANDUM

for the [redacted]

Bureau of Ships, Department of the Navy

INVESTIGATION OF A $\frac{1}{5}$-SCALE MODEL OF A PROPOSED HIGH-SUBMERGED-SPEED SUBMARINE IN THE LANGLEY FULL-SCALE TUNNEL

By Stanley Lipson, Bennie W. Cocke, and
William I. Scallion

Langley Aeronautical Laboratory
Langley Air Force Base, Va.

CLASSIFICATION CHANGE

To [redacted] UNCLASSIFIED + LIMITATION ADDED

By authority of NASA CCN 233 DTD JAN. 1-31, 1976

Changed by .... SAM ...... Date 7-2-81

CLASSIFICATION CHANGE

Limitation removed NASA ID 71-67 (1-11-71)

NATIONAL ADVISORY COMMITTEE
FOR AERONAUTICS
WASHINGTON

[redacted]

NATIONAL ADVISORY COMMITTEE FOR AERONAUTICS

RESEARCH MEMORANDUM

for the

Bureau of Ships, Department of the Navy

INVESTIGATION OF A $\frac{1}{5}$-SCALE MODEL OF A PROPOSED HIGH-SUBMERGED-SPEED SUBMARINE IN THE LANGLEY FULL-SCALE TUNNEL

By Stanley Lipson, Bennie W. Cocke, and
William I. Scallion

SUMMARY

The results of an investigation to determine the drag, static stability, control effectiveness, boundary-layer conditions, and first-order effects of propeller operation on a $\frac{1}{5}$-scale model of a proposed high-submerged-speed submarine with various bridge-fairwater and tail configurations are presented. The model hull was a body of revolution 30.66 feet in length and had a fineness ratio of 5. All data were obtained at a Reynolds number of approximately 22,300,000 based on model length.

The drag of the complete scheme-2 model configuration (large bridge fairwater and rearward-located tails) was approximately 63.5 percent higher than the drag of the basic clean hull. The flooding and venting openings were responsible for approximately 14.4 percent of the drag of the complete configuration, and the complete model drag was approximately 9 percent lower with the alternate appendages (minimum bridge fairwater and forward-located tails) installed.

The model was statically unstable for all configurations investigated in pitch and in yaw. The scheme-2 (rearward-located) tail with the large stabilizer produced the largest stabilizing moment; however, on the basis of comparable areas, the forward-located tail was more effective for the propeller-removed condition. The effect of propeller operation was to increase the stability and control effectiveness for the rearward-located tails, which were influenced by the slipstream.

For the forward-located-tail arrangement, located ahead of the propeller, only minor effects were indicated.

Boundary-layer and wake surveys at the stern of the model indicated that the propeller was completely immersed in the low-energy wake but did not show any extreme asymmetry in the flow at the propeller location.

INTRODUCTION

A general research program is in progress to determine a design for a submarine with efficient submerged high-speed operation. Basic studies of hull forms (reference 1) and surface openings, as well as tests of specific model configurations, have been conducted in water tanks at David Taylor Model Basin and Stevens Institute as part of this program. In general, the models used in these tests were small scale and it was not possible to duplicate details such as double hull construction, flood- and vent-hole arrangement, and internal compartmenting that would exist on the full-scale submarine. It was desirable, therefore, to evaluate carefully the drag and aerodynamic characteristics of a large-scale model incorporating as many details as possible.

A $\frac{1}{5}$-scale model of the proposed submarine has been tested in the Langley full-scale tunnel at the request of the Bureau of Ships, Department of the Navy. The test program included: (1) force tests to determine the drag, control effectiveness, and static stability characteristics for a number of model configurations, both in pitch and in yaw, (2) pressure measurements to determine the boundary-layer conditions and flow characteristics over the rear of the model and in the region of the propeller, and (3) an investigation of the effects of propeller operation on the model aerodynamic characteristics.

This paper presents the complete results of these tests along with pertinent analyses and includes all the data previously presented in data report form (reference 2). All test results were obtained at a Reynolds number of approximately 22,300,000 based on model length.

SYMBOLS AND COEFFICIENTS

The symbols and coefficients used in the presentation of data were chosen in accordance with one of the standard systems given in reference 3. All moment coefficients presented have been computed about a point on the model which corresponds to the full-scale submarine center-of-gravity location specified by the Bureau of Ships as 9.05 feet forward

of the midlength point and 1.39 feet below the hull center line. Figure 1 illustrates the force and moment convention used in this paper.

D'	drag coefficient	$\left(\frac{D}{\frac{1}{2}\rho l^2 U^2}\right)$
Y'	lateral-force coefficient	$\left(\frac{Y}{\frac{1}{2}\rho l^2 U^2}\right)$
K'	rolling-moment coefficient	$\left(\frac{K}{\frac{1}{2}\rho l^3 U^2}\right)$
M'	pitching-moment coefficient	$\left(\frac{M}{\frac{1}{2}\rho l^3 U^2}\right)$
N'	yawing-moment coefficient	$\left(\frac{N}{\frac{1}{2}\rho l^3 U^2}\right)$

D	drag force in direction of relative flow, pounds
Y	lateral force component, positive for force acting to starboard, pounds
K	rolling moment, positive when acting to produce heel to starboard, foot-pounds
M	pitching moment, positive when acting to produce positive pitch (nose up), foot-pounds
N	yawing moment, positive when acting to produce yaw to starboard, foot-pounds
ρ	mass density of air, pound-second^2/feet^4
U	free-stream velocity, feet per second
l	length of body, feet
u	local velocity, feet per second
α	angle of attack, positive nose up, degrees
ψ	angle of yaw, positive nose to starboard, degrees

δ_r rudder angle, positive when trailing edge deflected to port, degrees

δ_s stern plane angle, positive when trailing edge deflected down, degrees

R Reynolds number $\left(\frac{\rho l U}{\mu}\right)$

P static-pressure coefficient $\left(\frac{p - p_o}{q_o}\right)$

p local static pressure, pounds per square foot

p_o free-stream static pressure, pounds per square foot

q_o free-stream dynamic pressure, pounds per square foot $\left(\frac{\rho U^2}{2}\right)$

μ absolute viscosity of air, pound-seconds per square foot

q local dynamic pressure, pounds per square foot $\left(\frac{\rho u^2}{2}\right)$

δ_{dr} bridge-fairwater dorsal rudder angle, positive when trailing edge deflected to port, degrees

MODEL

The $\frac{1}{5}$-scale model used in these tests was constructed to duplicate as closely as possible the details of double hull construction, such as bulkhead location and margin plate installation as shown on Bureau of Ships drawings for the full-scale submarine. Drawings and photographs of the various configurations tested are shown in figures 2 to 9.

The basic body was a body of revolution having a length of 30 feet 8 inches and a maximum diameter of 6 feet $1\frac{1}{2}$ inches. Flood and vent holes placed in the skin of the external hull and bulkheads between the external and internal hull corresponded closely in number and location to those specified for the full-scale submarine. The bulkheads located as shown in figure 2 divided the area between the external and internal hulls into compartments so that flow from one compartment to another was prevented. The margin plates, also indicated on figure 2, ran longitudinally the length of the flood compartments and prevented flow between the ballast tank area and free-flooding area. Vent and flood

holes in the outer hull were arranged so that the number of holes, hole locations, and total hole area per compartment corresponded closely to the full-scale specifications. A typical section indicating flood- and vent-hole locations is shown in figure 2(b). The basic body with all flood and vent holes open is subsequently referred to as the "operational hull."

The complete scheme-2 configuration (Bureau of Ships designation) consisted of the operational hull with a large bridge fairwater and aft-located cruciform tail arrangement. The other two tail configurations investigated consisted of, (1) the scheme-2 vertical tail combined with a horizontal tail of smaller area than the scheme-2 horizontal tail, and (2) a forward-located tail arrangement of different plan form than the scheme-2 tail. A smaller bridge fairwater subsequently referred to as the "minimum bridge fairwater" replaced the scheme-2 bridge fairwater for some of the tests. Figure 2(c) shows the general arrangements of the various model configurations as well as the areas of the different tails investigated.

The propeller used for some of the tests was a 26-inch-diameter model of a four-blade standard-type aircraft propeller, and was located as indicated in figure 6 on the stern of the model.

METHODS AND TESTS

The model was mounted for test on the six-component balance system in the Langley full-scale tunnel using a two-strut mounting system to minimize strut interference (fig. 3).

Initial force tests were made to determine the aerodynamic characteristics of the clean hull with all openings sealed and faired and with all appendages removed. Successive tests were then made, as the operational components of the submarine were installed, to determine the effects of flood and vent openings, tail surfaces, and bridge-fairwater arrangements on the model characteristics. In addition to these force tests, measurements were also made to determine the effectiveness of the controls. All model configurations were tested through a pitch range of $\pm 6^{\circ}$ and three model configurations were also studied through a yaw range from -3° to 9°. In conjunction with the force tests, the flow about the model was studied by visual observation of wool tufts attached to the surface of the model and by boundary-layer and wake pressure measurements at several stations along the aft portion of the model and in the region of the propeller.

A few tests were made with an aircraft type of propeller installed to determine the first-order effects of propeller operation on static

stability, control effectiveness, and flow conditions at the rear of the model. For these tests the propeller was operated at thrust coefficients approximating high-speed conditions as determined by setting thrust equal to model drag (at $\alpha = 0^{\circ}$).

All tests were made at a tunnel speed of approximately 78 miles per hour which corresponds to a Reynolds number of 22,300,000 based on model length. All data have been corrected for the effects of strut tares, tunnel buoyancy, and blocking.

RESULTS AND DISCUSSION

Drag

The results of the drag investigation are summarized in table I and drag polars for three of the test configurations are shown in figure 10. These results indicate that the drag of the complete scheme-2 configuration ($D' = 0.00188$) is 63.5 percent higher than the drag of the basic hull ($D' = 0.00115$). This drag-coefficient increase of 0.00073 is composed of increments of 0.00028 for the rear tail installation (fig. 6), a total of 0.00027 for all flooding and venting openings (figs. 4 and 5), and 0.00018 for the scheme-2 bridge fairwater (fig. 9). Tests of the minimum bridge-fairwater and forward-located tail installations (figs. 4 and 8) show that the complete model drag would be reduced approximately 9 percent with these alternate appendages installed. It should be noted that, although a careful evaluation of strut tares was made for the model, it was not feasible to determine the influence of the support struts on the drag increments measured for the ballast-tank flood holes along the bottom of the model and the increments measured for these holes may, therefore, be somewhat low. Despite the low increments indicated for these ballast-tank flood holes, the total drag of 0.00027, charged to all flood and vent openings, represents approximately 14.4 percent of the complete scheme-2 model drag ($D' = 0.00188$).

The detailed flow studies in the junctures of the bridge fairwaters and the tail assemblies indicated that, except at the blunt afterbody of the minimum bridge fairwater, no separation tendencies were evident. The attempt to reduce the drag of the scheme-2 rear tail configuration by extending the chord and reducing the trailing-edge angle of the thick inboard strut and by filleting the sharp step juncture (compare figs. 6 and 7) did not result in any appreciable reduction. This result is attributed to the fact that the greater portion of this section of the tail was enveloped by the thick boundary layer of the hull.

Longitudinal Stability

In the ensuing discussion, the usual interpretation of the wind-tunnel data has been made and the external aerodynamics of the model have been treated as the prime factors determining the model's static-stability characteristics. It is realized, though, that in order to obtain a more realistic picture of the submarine's "flying qualities" these static-stability results must be considered with other factors, such as the effect of the metacentric height which may be of first-order importance in the dynamics of the submarine. Any analysis of the submarine's dynamic stability, however, is beyond the intended scope of this paper.

Effect of the appendages.- As shown in figure 11, the operational hull was statically unstable through the pitch range investigated and, while the addition of the various horizontal tail surfaces afforded some improvement in stability, none of the arrangements tested resulted in a statically stable configuration. The amount of stability provided by the tail surfaces is probably more truly represented in the negative angle-of-attack range where the tail was less affected by the rear mounting strut. The forward-located horizontal tail is more effective than the rear tail configuration with small horizontal surfaces installed. Although the areas are practically equal, the forward tail gave about 25 percent more stability, even though the tail length from the center of gravity is about 10 percent greater for the rearward-located tail.

Tests in yaw of the large rearward-located horizontal surface and the forward-located tail (fig. 12) showed yaw to have practically no effect on the static longitudinal stability of the model. The nose-up trim shift, occurring with increased positive yaw, was slightly greater for the rearward-located tail than for the forward-located horizontal tail.

The effect on the model's longitudinal stability resulting from the addition of the two different bridge fairwaters is shown in figure 13. At zero yaw, the scheme-2 bridge fairwater gave a constant increment of pitching-moment coefficient $\Delta M'$ of +0.0002 throughout the pitch range investigated. This increment increased with yaw and at a yaw angle ψ of 9.2° varied from $\Delta M' = +0.00035$ to $+0.00075$ while the minimum bridge fairwater gave $\Delta M' = +0.0002$.

Effect of control-surface deflection.- In the pitch range investigated (5.7° to -6.3°), angle of attack had little influence on the variation of pitching-moment coefficient with control-surface deflection for the two rearward-located tail arrangements (figs. 14(a) and 14(b)). The slopes of the curves of M' against δ_s ($\partial M'/\partial \delta_s$ of approximately -0.0001 for the large rearward-located tail and -0.00005 for the small

rearward-located tail) remain approximately constant up to a deflection of about 15° and then are reduced by the separation over the controls at high deflections. The tests of the forward-located tail surface were conducted over a greater pitch range (9.7° to -8.3°) than the rearward-located surfaces and at the higher angles of attack showed a large loss in effectiveness past deflections of 15° (fig. 14(c)). The slope of the curve of M' against δ_s $\left(\frac{\partial M'}{\partial \delta_s} = -0.00008 \text{ at low deflections}\right)$ increased up to a deflection of 15° but for the low angle-of-attack range was only moderately reduced at the higher deflections. Figure 15 affords a rapid comparison of the relative characteristics of the three surfaces at $\alpha = 0.3°$ with the propeller removed.

Effect of power.- The effect of propeller operation on the longitudinal stability for the three horizontal-tail arrangements with zero control-surface deflection is presented in figure 16. Inasmuch as the boundary layer in the region of the forward-located surface was not materially influenced by propeller operation, the negligible change in the variation of M' with α for this surface, due to propeller operation, may be considered the normal-force effects of the propeller. In the case of the large rearward-located horizontal tail, however, approximately 15 percent of the total surface area is located directly aft of the propeller so that the stabilizing effect of the propeller operation is greater than that due only to the normal-force effects. With the propeller operating and for the pitch range investigated, angle of attack had no effect on the slope of the curves of M' against δ_s for the large rearward-located horizontal surface (fig. 17). The comparison of the relative effectiveness of the forward-located tail and the large rearward-located horizontal surface previously given is considerably altered when power is considered. As illustrated by figure 18, where the propeller-removed curve for the forward-located tail may be considered as equivalent to its expected propeller-operating characteristics, it is evident that the large rear control surface has approximately 50 percent greater effectiveness for the propeller-operating condition.

Lateral Stability

Effect of the appendages.- The variations of yawing-moment coefficient N', rolling-moment coefficient K', pitching-moment coefficient M', and lateral-force coefficient Y', with angle of yaw are presented in figure 19 for five different appendage arrangements on the operational hull. The model configurations were selected so that the effects in yaw of the rearward-located (scheme-2) fin and rudder, the forward-located fin and rudder, the scheme-2 bridge fairwater, and the minimum bridge fairwater may be separated and analyzed, either alone

or for various operational arrangements. The destabilizing effect of the large scheme-2 bridge fairwater on the lateral stability characteristics is quite evident from the data presented in figure 19. As shown, the characteristics in yaw of the two fin and rudder configurations, which have nearly equal areas, are very similar with the movable surfaces set at zero deflection.

The effect of pitch at various yaw angles on the yawing-moment-coefficient characteristics of the two tail arrangements is presented in figure 20. Except at the higher angles of yaw, there is little variation in N' with angle of attack.

Effect of control-surface deflection.- At zero yaw, angle of attack has little effect on the variation of N' with rudder deflection for the rearward-located tail (fig. 21(a)) but does result in a trim shift at the higher angles of yaw. The effectiveness of the rearward-located (scheme-2) fin and rudder tends to decrease somewhat more rapidly with increasing δ_r for the higher yaw angle, $\psi = 9.2^\circ$, and at this yaw the model could not be trimmed. The influence of angle of attack is approximately the same for the forward-located tail (fig. 21(b)) as noted for the rearward arrangement. For the forward-located fin and rudder, however, the effectiveness increases at the higher δ_r's and trim was almost attained at $\psi = 9.2^\circ$ at the maximum surface deflection.

The effect on the lateral characteristics of deflecting the large (scheme-2) bridge-fairwater dorsal rudder (fig. 9) is shown in figure 22. The dorsal rudder was operated as a spoiler, with its prime purpose being to reduce the lift produced by the bridge fairwater in yaw. The result of its action on eliminating the rolling moment due to the bridge fairwater in yaw is presented in figure 22(a). For -0.3° and low negative pitch angles, the effectiveness was approximately the same at $\psi = 6.2^\circ$ as at zero yaw and almost full deflection of the dorsal rudder was required to trim at $\psi = 6.2^\circ$. At an angle of attack of 3.7°, however, trim could not be obtained for a yaw of 6.2° and no further effectiveness was attained past $\delta_{dr} = 10^\circ$.

At $\psi = 0^\circ$ and $\delta_{dr} = 0^\circ$, the large bridge fairwater, considered as a lifting surface, is at zero lift and the angle of attack of the submarine, that is, yaw of the lifting surface, does not appear to have any effect on the fairwater's resultant lift for the pitch range investigated. With increased dorsal-rudder deflection and, therefore, some increase in loading, the bridge-fairwater yawing-moment and side-force contribution is more sensitive to changes in pitch of the model (figs. 22(b) and 22(d)). At a yaw of 6.2°, the negative deflection of the dorsal rudder tends to reduce the lift loading and, thus, when $\delta_{dr} = -40^\circ$ is reached, the lift loading has been so reduced that the submarine's angle of attack again has a small effect on the N' and Y'

induced by the scheme-2 bridge fairwater. The pitching-moment coefficient shows practically no effect due to deflection of the dorsal rudder (fig. 22(c)).

Pressure Investigation

Hull pressure distribution.- The variation with yaw of the surface static-pressure distribution obtained along the starboard-side center line of the model is shown in figure 23. These results do not show any tendency for flow separation as indicated by the moderate adverse pressure gradient at the rear of the model. The variation in magnitude of peak pressure with yaw is small for the yaw range shown, although a definite forward shift in center of pressure with increasing yaw is indicated, which produces the high degree of static instability for the basic hull previously shown by force tests. It should be pointed out that the irregularity in the pressure distribution, occurring approximately $2\frac{1}{2}$ feet aft of the nose, is caused by a slight discontinuity in the hull surface where the nose section, which was readily removable for maintenance purposes, joined the main part of the hull.

Boundary-layer surveys.- Surveys were taken at three different longitudinal positions ($0.80l$, $0.88l$, and $0.96l$) along the center line, both on the upper surface and on the starboard side of the hull. The effect of angle of attack on the boundary-layer flow of the basic hull configuration is illustrated in figures 24 and 25. In general, the boundary-layer thickness increased with increasing positive pitch and with rearward position along the hull. The highest flow retardation was evident in the survey taken at the higher angles of attack, either positive or negative, at the $0.96l$ station along the starboard side (fig. 25(c)). Flow studies, made by means of tufts attached to the hull, showed a tendency for the flow at the aft end of the hull, at positive pitch angles, to curve downward from the upper surface, over the sides, and toward the lower pressure region of the under surface.

The same effect due to pitch was noted for the flow over the operational hull (fig. 26), as was discussed for the basic hull, although the variation of the velocity profiles for the various angles of attack considered was not as great for the operational hull as for the basic configuration. The tendency for the velocity distributions obtained on the rear of the operational hull along the upper-surface center line, to become asymptotic to a u/U of 0.95, is probably due to wake effects of the large (scheme-2) bridge fairwater.

The effect of hull condition is shown in figure 27. It is believed that the higher energy flow obtained in the first 6 inches above the skin

for the operational hull (fig. 27) is due to the effects of turbulence induced in the boundary layer by the venting slots on the hull upper surface (fig. 4). As would be expected, the effect of propeller operation (fig. 28) is to increase the velocity in the region close to the propeller location.

Wake surveys.- The results of pressure surveys in the wake of the hull are shown in figure 29 for the scheme-2 fin and rudder with the large horizontal tail installed and in figure 30 for the forward tail-surface arrangement. For the former configuration, two survey locations were investigated, one at the propeller location and one 9 inches aft of the propeller location. These results are presented as contour plots showing lines of constant ratios of local dynamic pressure to free-stream dynamic pressure with the measured local static pressure coefficients indicated throughout the wake.

The q/q_o distributions for the two different tail configurations were very similar at the station 9 inches behind the propeller and the values were slightly higher than the pressures measured at the propeller location. The distortion shown in the lower portion of the pressure distributions of figures 29 and 30 is due to interference effects of the tail-strut wake. These results indicate that the complete propeller will be operating in the hull wake but do not show any extreme asymmetry in the flow entering the propeller location.

Propulsive Efficiency

Although the propeller used during the tests was a standard type of aircraft propeller which, when operating at the thrust-equal-drag condition for these tests was not operating at its peak efficiency, propulsive efficiencies of the order of 93 percent were obtained with the various tail configurations investigated. These high propulsive efficiencies obtained by operating the propeller at the stern, and thus converting the kinetic energy of the wake into useful work, have been indicated by the analysis presented in reference 4. A similar result in which a maximum propulsive efficiency of 92 percent was measured for the "thrust-equal-hull-drag" condition, was obtained in an unpublished investigation of a stern propeller arrangement on an airship model in the Langley 19-foot pressure tunnel.

CONCLUDING REMARKS

1. The drag of the basic hull form ($D' = 0.00115$) is increased 63.5 percent by the installation of the scheme-2 appendages and opening of the flooding and venting holes.

2. The flooding and venting openings contributed approximately 14.4 percent of the total drag of the scheme-2 model configuration ($D' = 0.00188$).

3. The drag of the complete model was reduced approximately 9 percent by the installation of the alternate appendages consisting of minimum bridge fairwater and forward-located tails.

4. The model was statically unstable in both pitch and yaw for all configurations investigated.

5. The forward-located tail surfaces had a lower drag, were more stabilizing, and produced more effective control than the comparable-area rearward-located surfaces for the propeller-removed condition.

6. The results of propeller-operating tests indicate that propeller operation had little effect on the stability or control effectiveness for the forward-located tail configuration, whereas an appreciable improvement in stability and control effectiveness was indicated for the rearward-located tails.

7. The bridge-fairwater dorsal rudder was relatively ineffective in reducing the rolling moment produced by the bridge fairwater in yawed attitudes. Approximately full deflection ($\delta_{dr} = 40^\circ$) was required to trim the rolling moment resulting at a yaw attitude of 6.2°.

8. Pressure measurements along the hull surface did not indicate any tendency for flow separation. A forward shift in center of pressure with yaw, indicated by these measurements, confirmed the instability of the basic hull previously shown by force tests.

9. The boundary-layer and wake surveys showed that the stern-located propeller was completely immersed in a low-energy wake region but did not indicate any extreme asymmetry in the flow at the propeller location.

Langley Aeronautical Laboratory
National Advisory Committee for Aeronautics
Langley Air Force Base, Va.

Stanley Lipson
Aeronautical Research Scientist

Bennie W. Cocke
Aeronautical Research Scientist

William I. Scallion
Aeronautical Research Scientist

Approved: Eugene C. Draley
Eugene C. Draley
Chief of Full-Scale Research Division

OMM

REFERENCES

1. Gertler, Morton: Resistance Experiments on a Systematic Series of Streamlined Bodies of Revolution - for Application to the Design of High-Speed Submarines. Rep. C-297, David Taylor Model Basin, Navy Dept., April 1950.

2. Cocke, Bennie W., Lipson, Stanley, and Scallion, William I.: Data from Tests of a $\frac{1}{5}$-Scale Model of a Proposed High-Speed Submarine in the Langley Full-Scale Tunnel. NACA RM SL50E09a, Bur. Ships, 1950.

3. Landweber, L., and Abkowitz, M. A.: A Proposed Nomenclature for Treating the Motion of a Submerged Body through a Fluid. Rev. ed., Dec. 1948. (Prepared for Committee on Nomenclature of the American Towing Tank Conference.)

4. Burgess, C. P.: Stern Propellers for Airships. Design Memo. No. 305, Bur. Aero., July 1938.

TABLE I

SUMMARY OF DRAG MEASUREMENTS

Test	Model configuration	D' at $\alpha = 0^\circ$	$\Delta D'$
1	Basic hull. Appendages removed; flood and vent openings sealed and faired	0.00115	-------
2	Same as 1 except scheme-2 rearward-located tail installed with the large horizontal surfaces	.00143	0.00028
3	Same as 2 except superstructure flooding and venting holes open aft of bulkhead 32	.00150	.00007
4	Same as 3 except superstructure flooding and venting holes open aft of bulkhead 4	.00161	.00011
5	Same as 4 except all superstructure flooding and venting holes open	.00165	.00004
6	Same as 5 except ballast tank flood holes open aft of bulkhead 32	.00168	.00003
7	Same as 6 except ballast tank flood holes open aft of bulkhead 4	.00168	-------
8	Same as 7 except all ballast tank and venting holes open (operational hull)	.00170	.00002
9	Same as 8 except minimum bridge fairwater installed	.00182	.00012
10	Same as 8 except scheme-2 bridge fairwater installed (complete scheme-2 configuration)	.00188	.00018
11	Same as 10 except fillets and fairings installed on scheme-2 tail surfaces	.00187	-.00001
12	Same as 10 except rearward-located (scheme-2) tail surfaces removed	.00160	-.00028
13	Same as 12 except scheme-2 rearward-located fin and rudder installed with the small horizontal surfaces	.00184	.00024
14	Same as 13 except forward-located tail surfaces installed	.00177	.00017

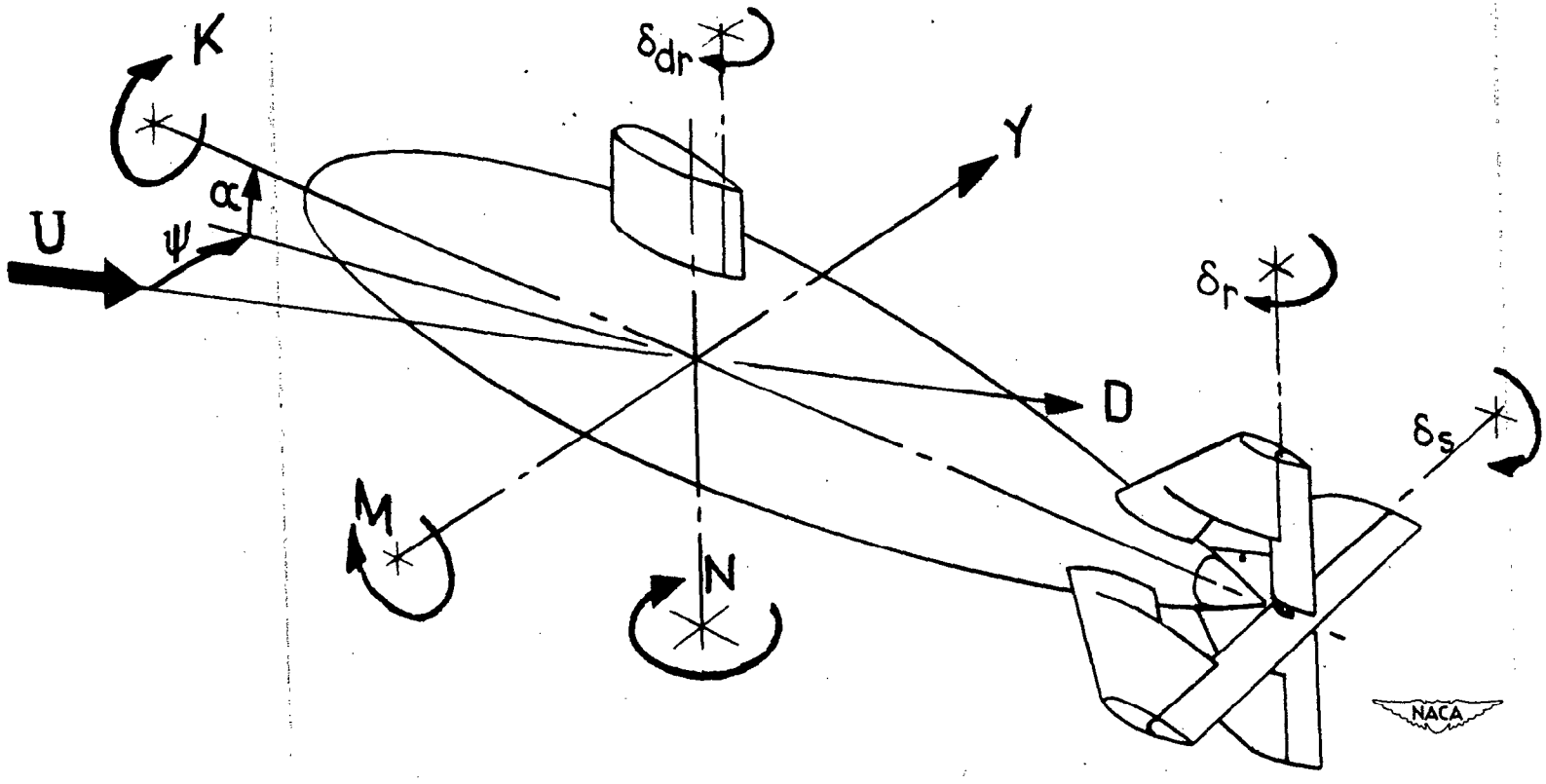

Figure 1.- The stability system of axes and sign convention. Arrows indicate positive directions of moments, forces, and control-surface deflections.

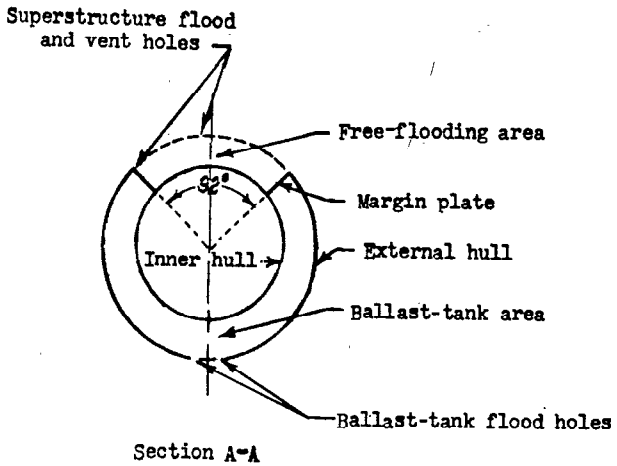

Model-External Hull Ordinates

Distance aft, ft	Radius ft	Distance aft, ft	Radius ft	Distance aft, ft	Radius ft
0	0	7.867	2.852	16.867	2.859
0.153	0.477	8.433	2.918	17.633	2.793
.383	.756	9.200	2.978	19.167	2.617
.767	1.053	9.967	3.016	20.700	2.412
1.533	1.476	10.733	3.046	22.233	2.164
2.300	1.779	11.500	3.062	23.767	1.873
3.067	2.025	12.175	3.067	25.300	1.549
3.833	2.228	13.033	3.062	26.833	1.176
4.600	2.397	13.800	3.041	28.367	.768
5.367	2.540	14.567	3.013	29.900	.304
6.133	2.663	15.333	2.975	30.667	0
6.900	2.762	16.100	2.924		

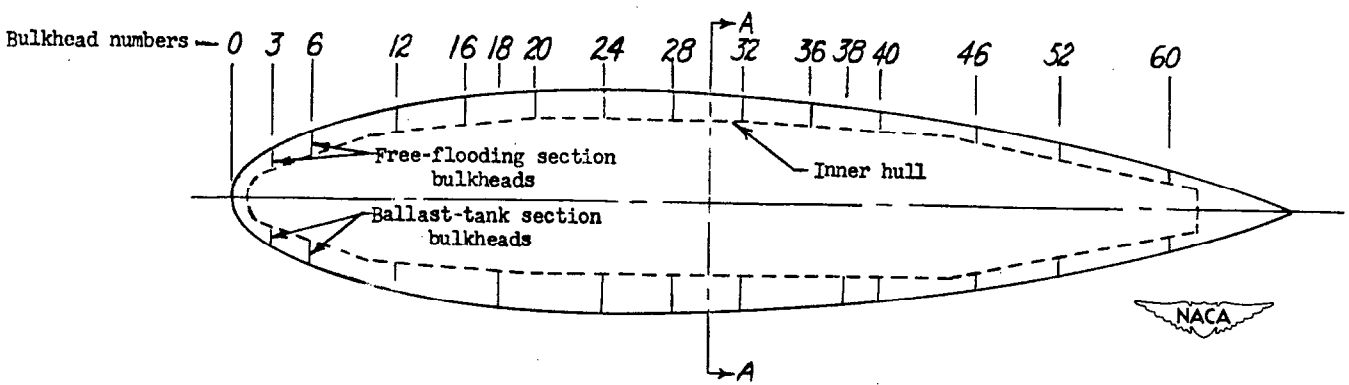

(a) General hull arrangement.

Figure 2.- Sketches of hull configurations.

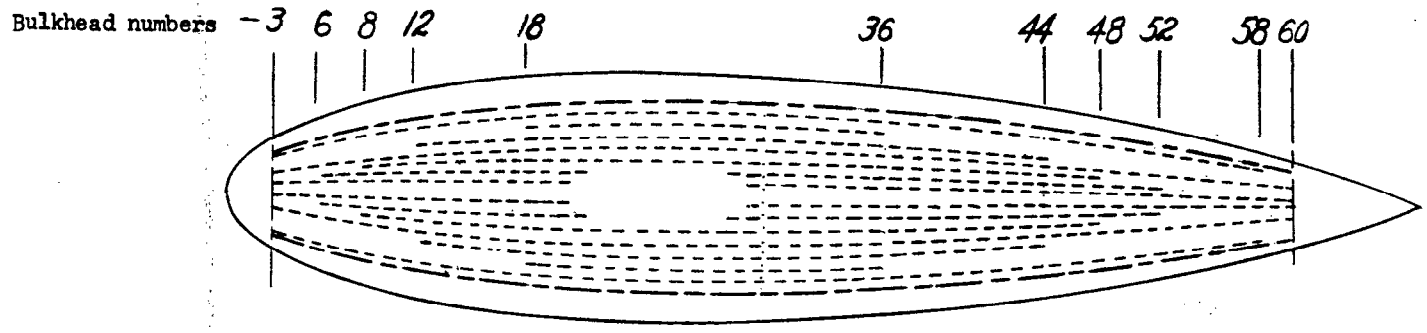

Top view of superstructure flood and vent-hole layout

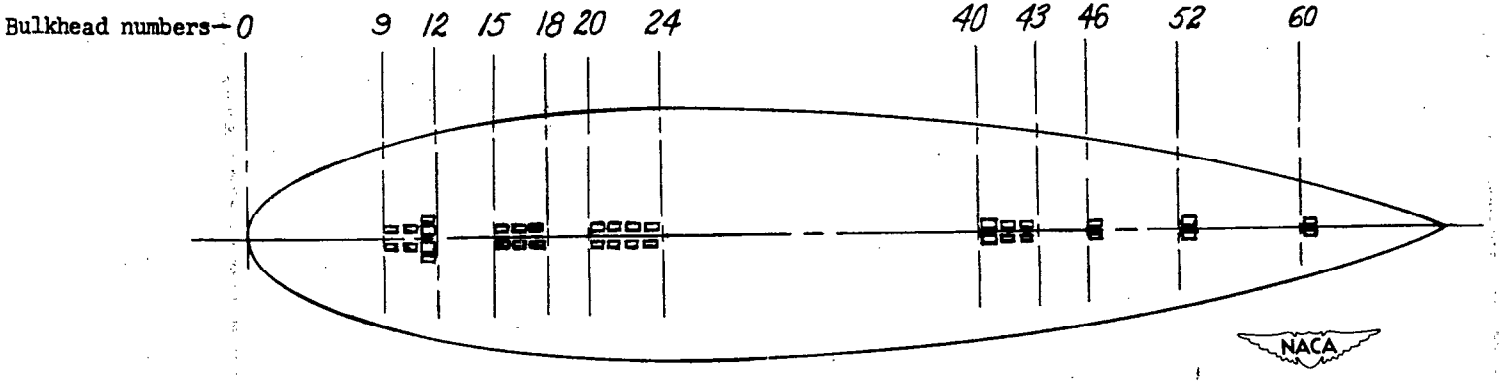

Bottom view of ballast-tank flood-hole layout

(b) Flood- and vent-hole arrangements.

Figure 2.- Continued.

Model tail surface areas (sq ft)		
Surface	Fixed area	Movable area
Scheme-2 large horizontal surfaces	8.80	4.48
Forward-located horizontal surfaces	4.32	4.12
Scheme-2 small horizontal surfaces	5.28	2.80
Scheme-2 vertical surfaces (fin and rudder)	7.36	3.36
Forward-located vertical surfaces (fin and rudder)	6.40	4.56

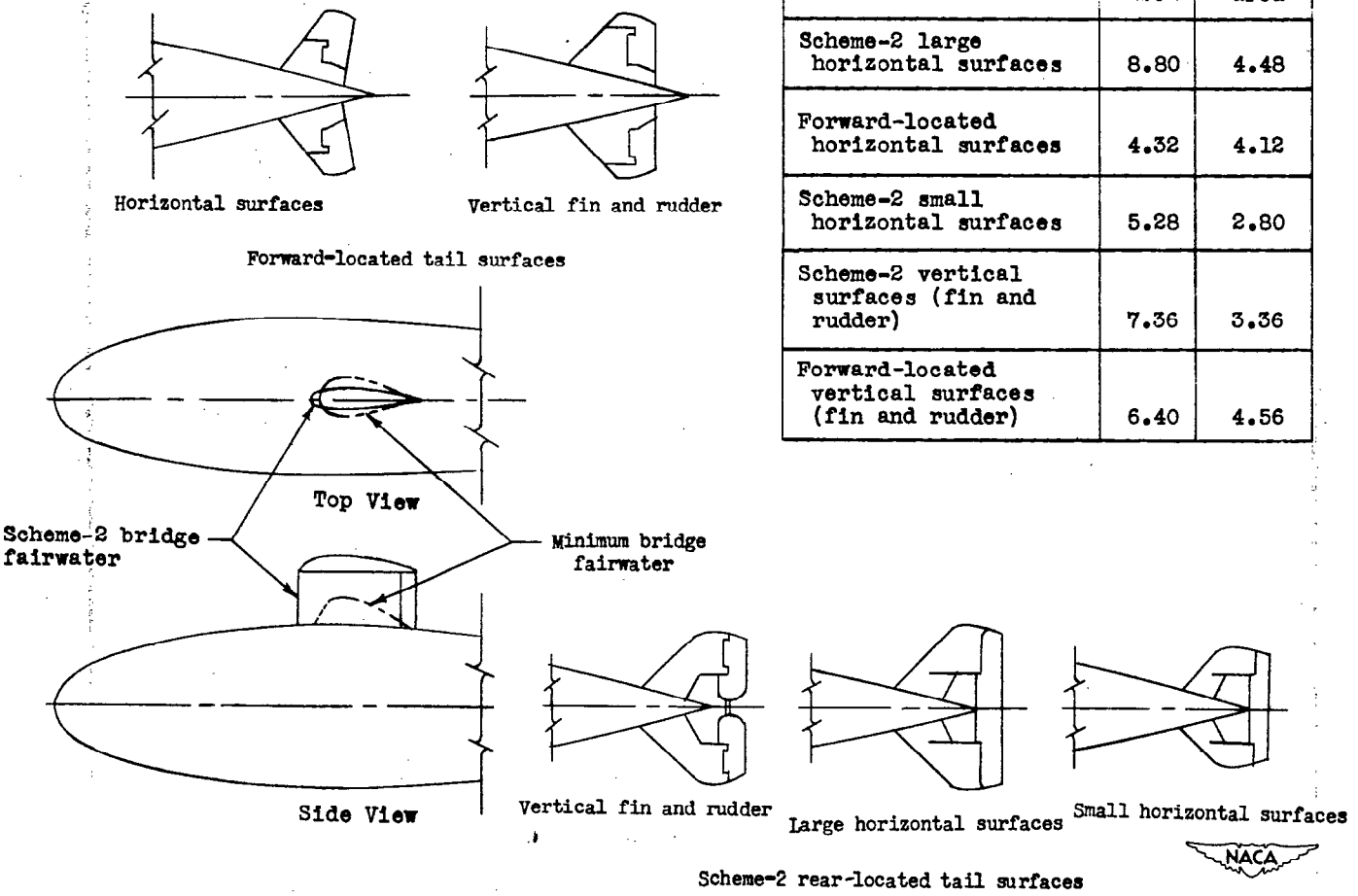

(c) Appendages.

Figure 2.- Concluded.

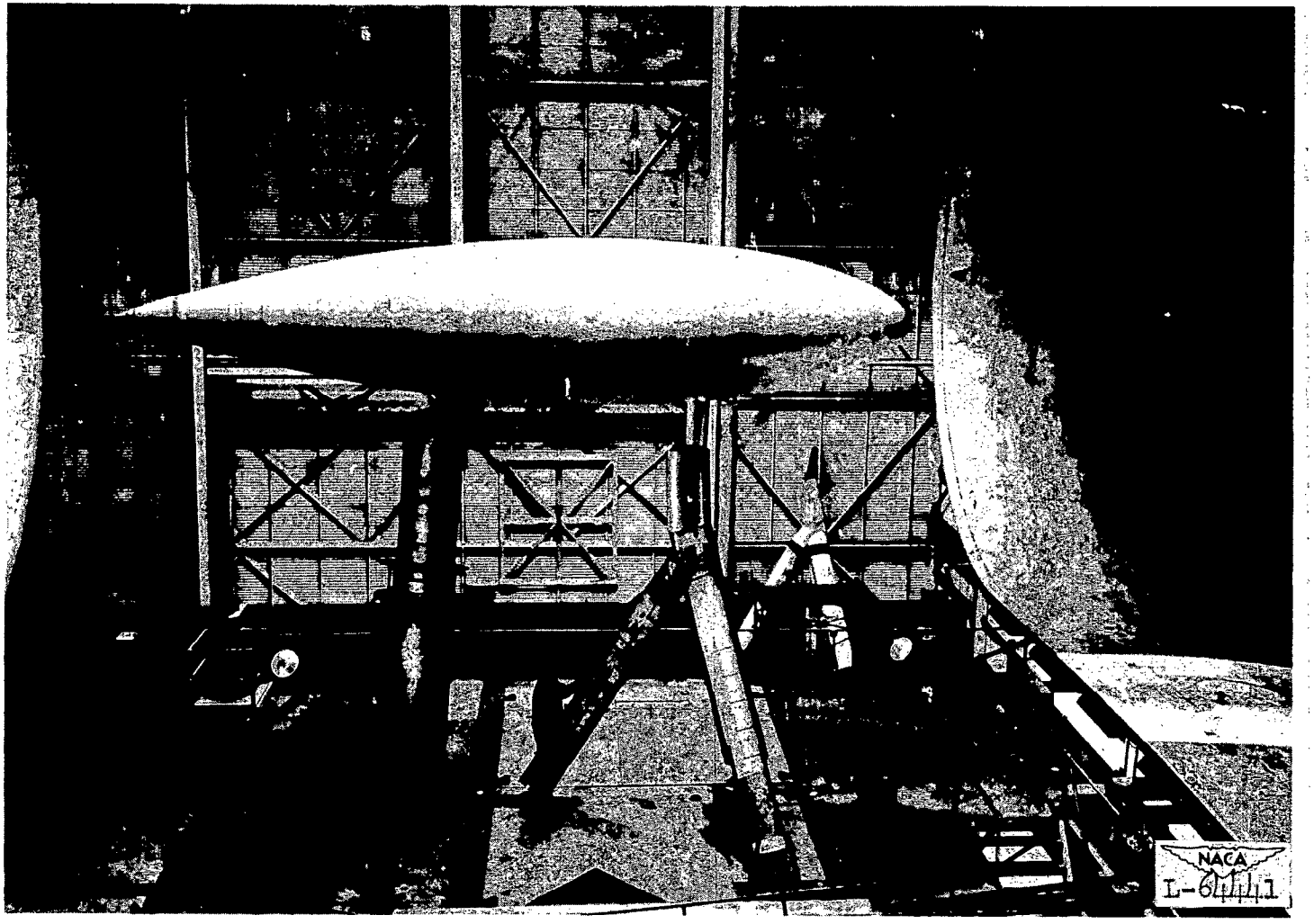

Figure 3.- General view of model in basic hull condition.

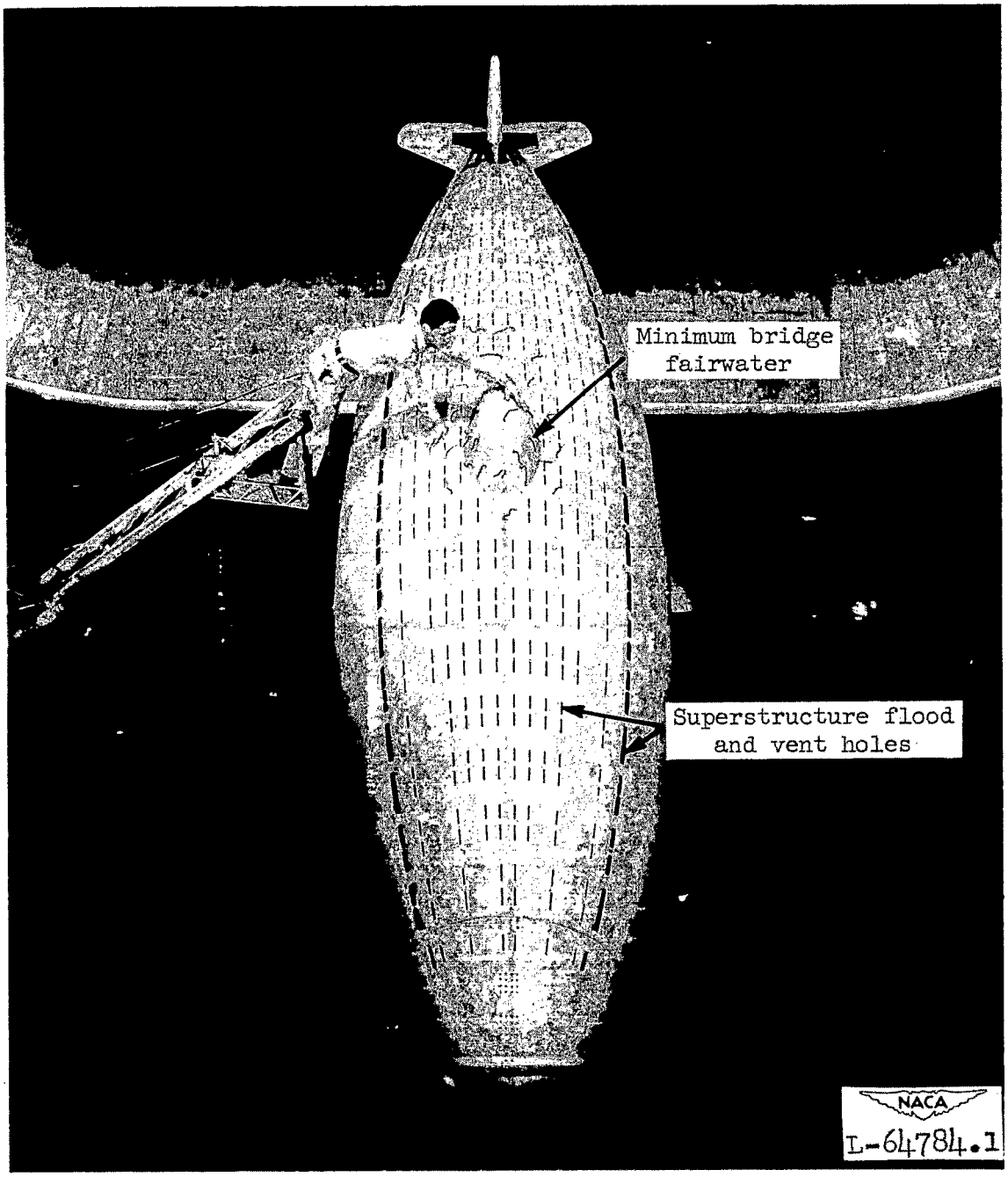

Figure 4.- Superstructure flooding- and venting-hole arrangement with minimum bridge fairwater installed.

Figure 5.- Main ballast-tank flood holes with scheme-2 bridge fairwater installed.

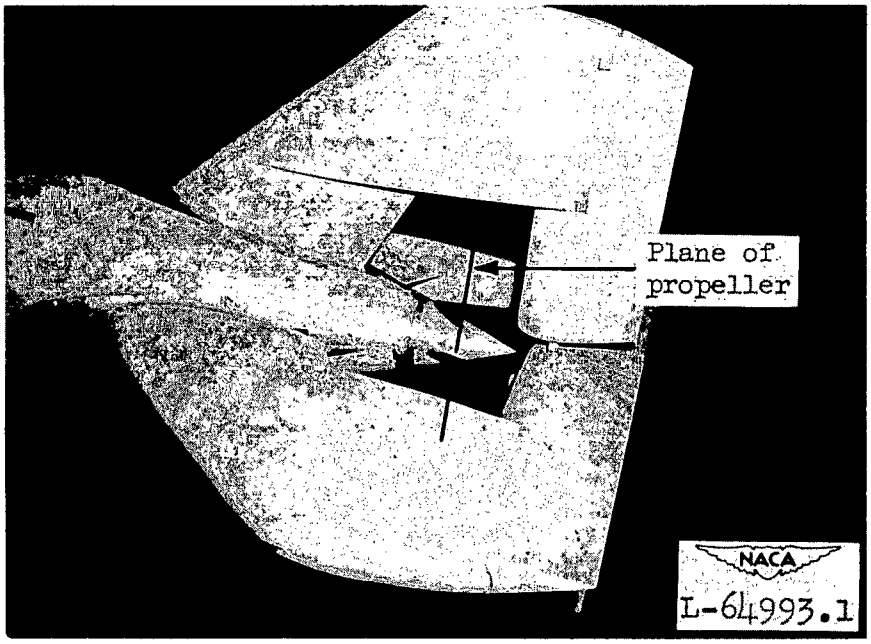

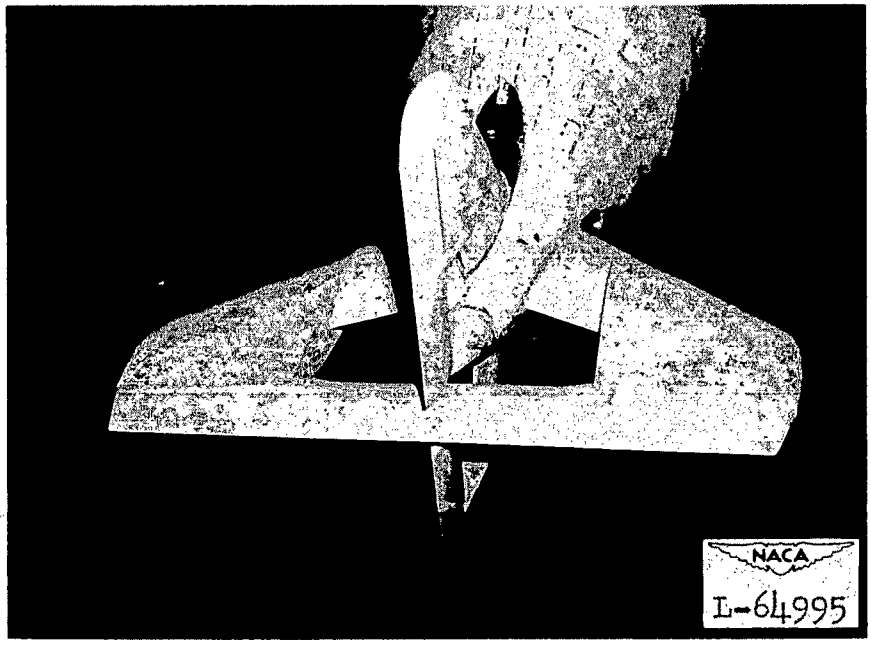

Figure 6.- Scheme-2 fin and rudder with large horizontal tail installed.

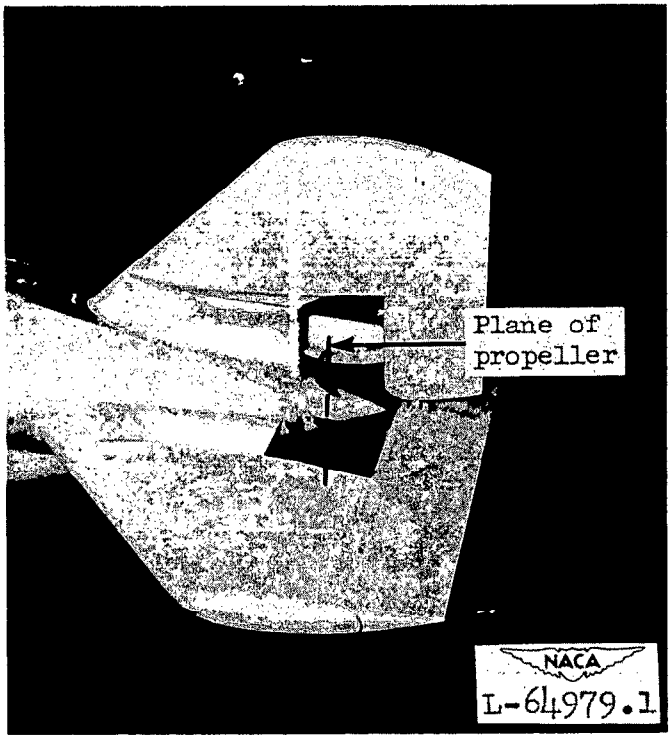

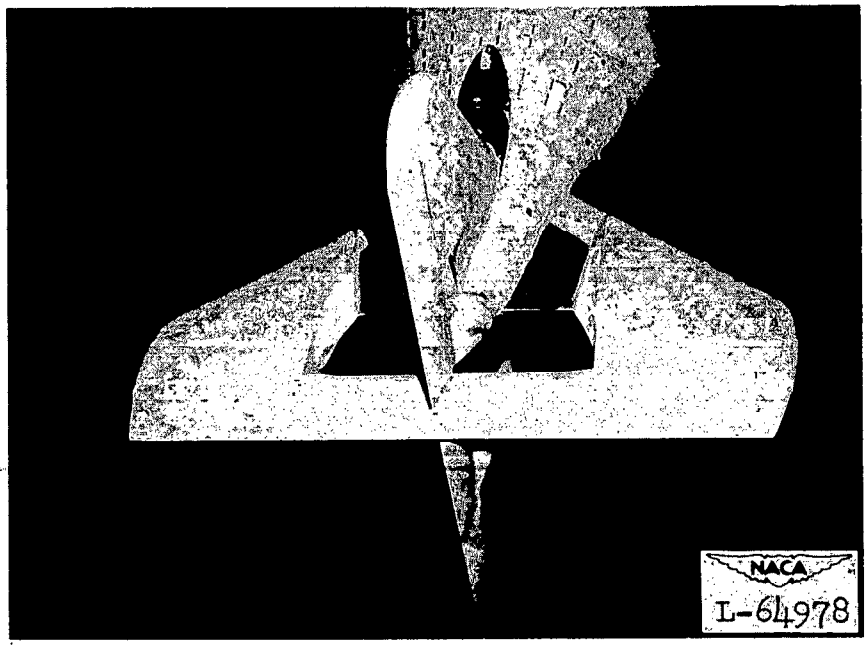

Figure 7.- Modified scheme-2 tail installation.

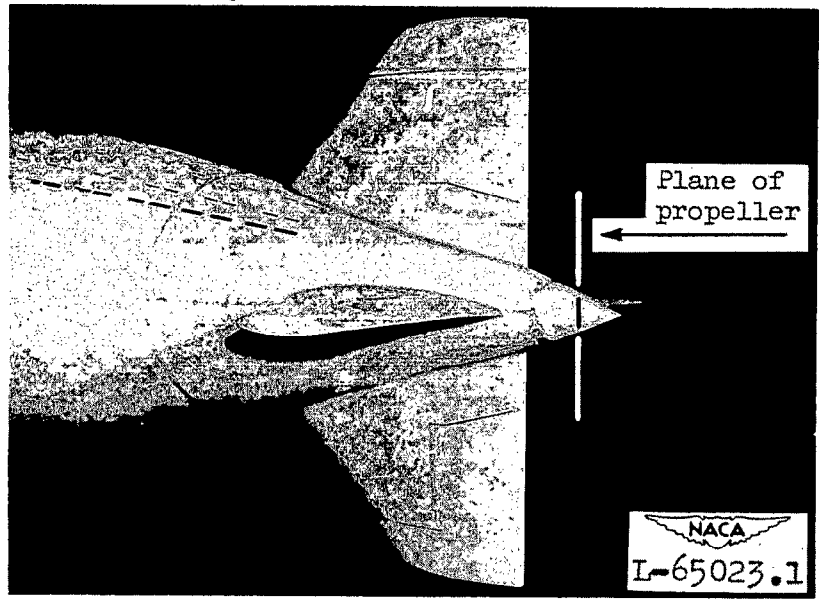

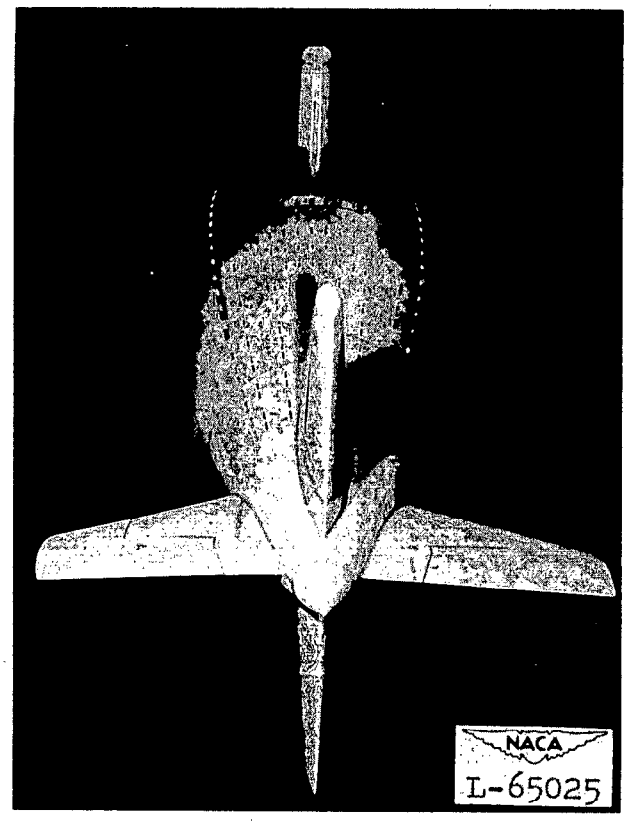

Figure 8.- Forward-located tail-surface arrangement.

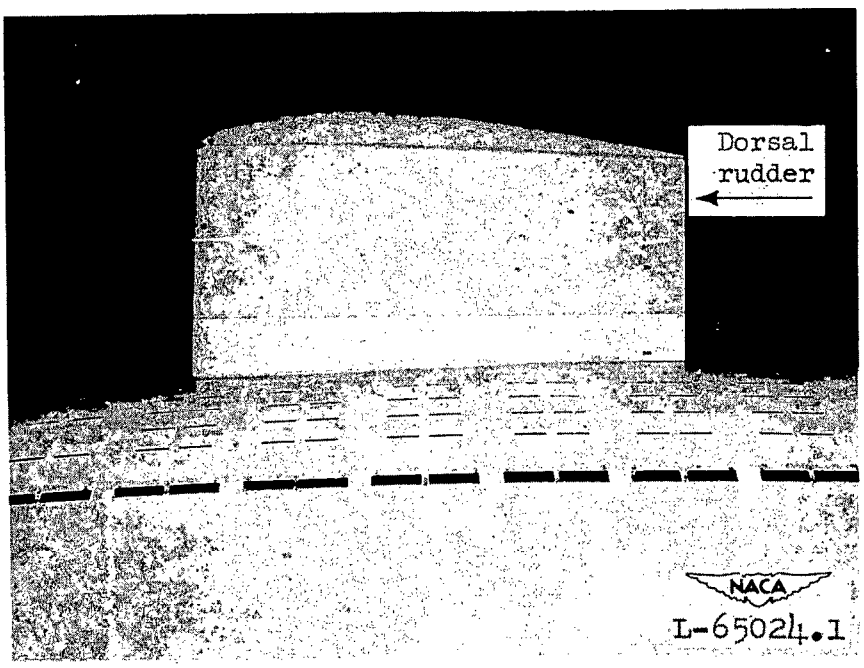

Figure 9.- Scheme-2 bridge fairwater.

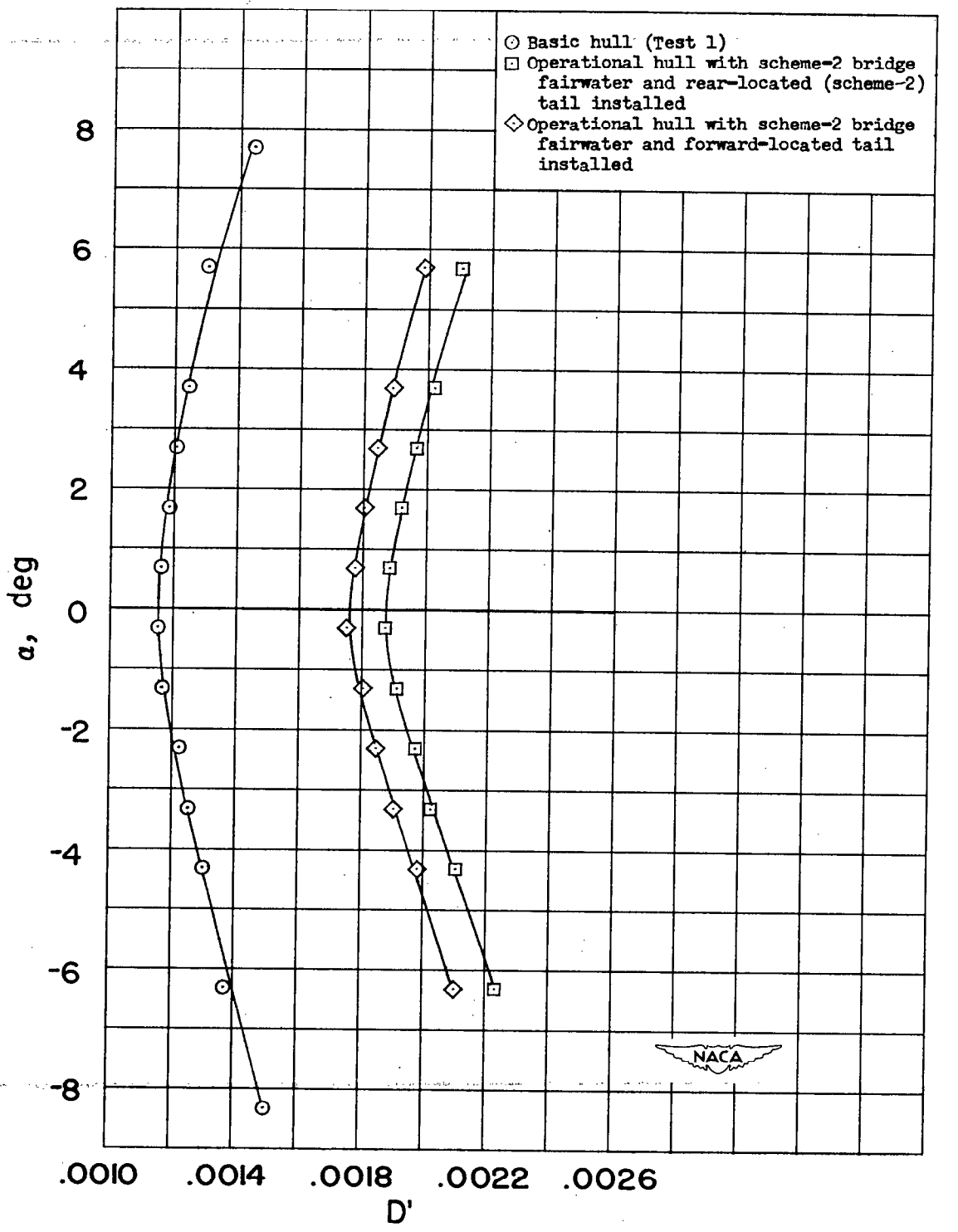

Figure 10.- Variation of drag coefficient with angle of attack for three model configurations. (See table I.) $\psi = 0^{\circ}$; $\delta_r = 0^{\circ}$; $\delta_s = 0^{\circ}$.

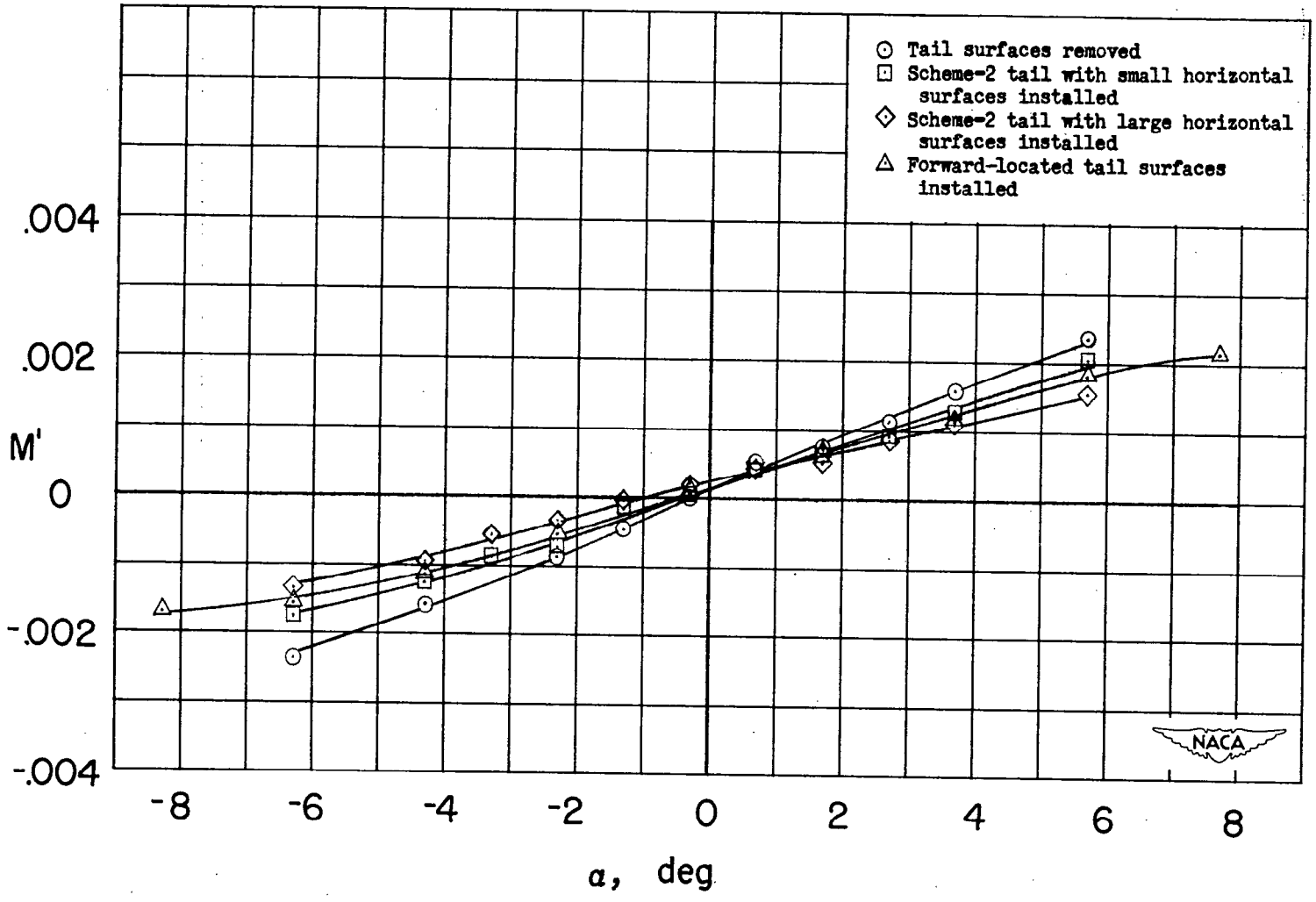

Figure 11.- Variation of pitching-moment coefficient with angle of attack for operational hull, including scheme-2 bridge fairwater, with and without tails installed. $\psi = 0^{\circ}$; $\delta_s = 0^{\circ}$; $\delta_r = 0^{\circ}$.

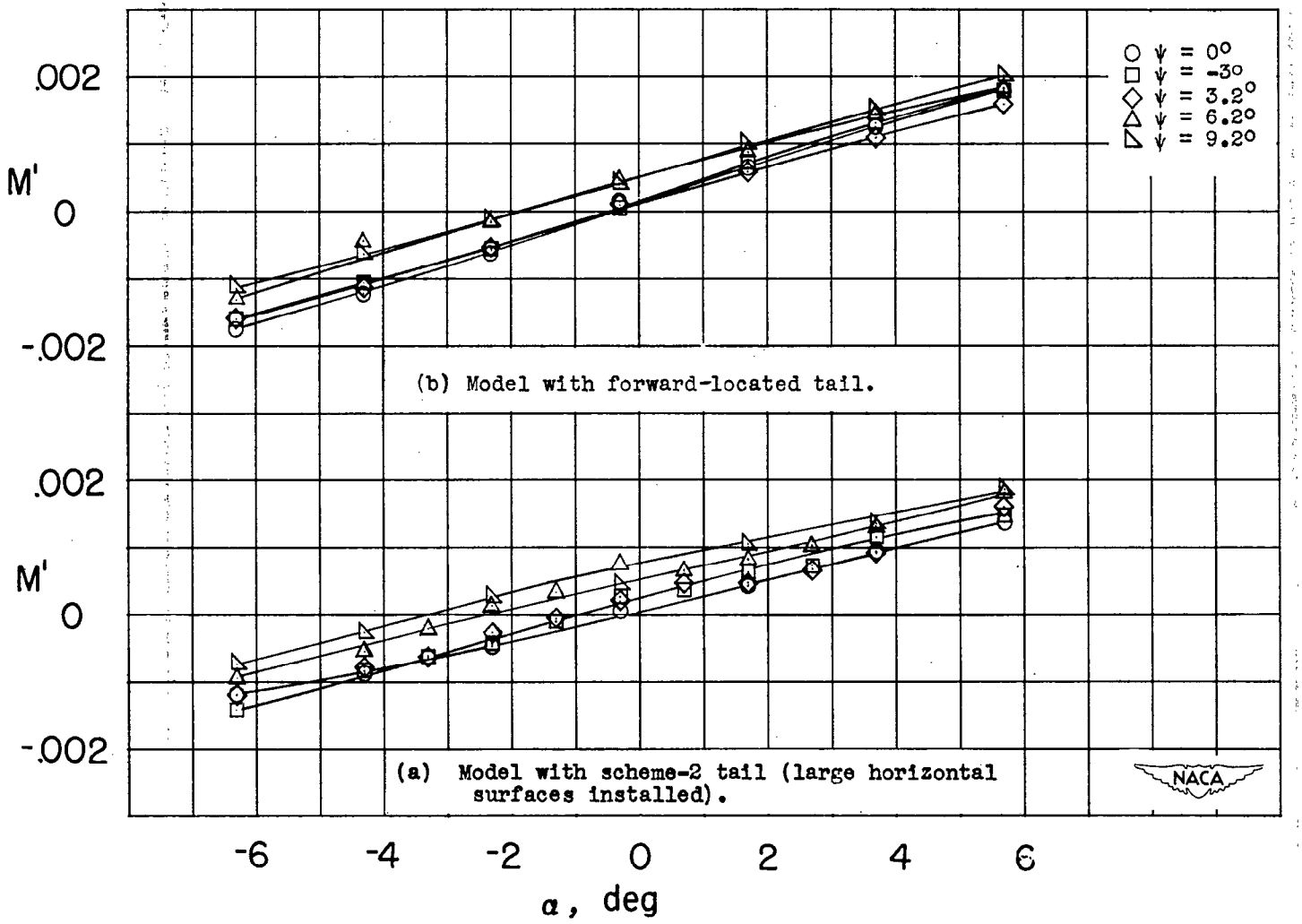

Figure 12.- Variation of pitching-moment coefficient with angle of attack and angle of yaw for the complete model with scheme-2 bridge fairwater installed. $\delta_r = 0^\circ$; $\delta_s = 0^\circ$.

CONFIDENTIAL

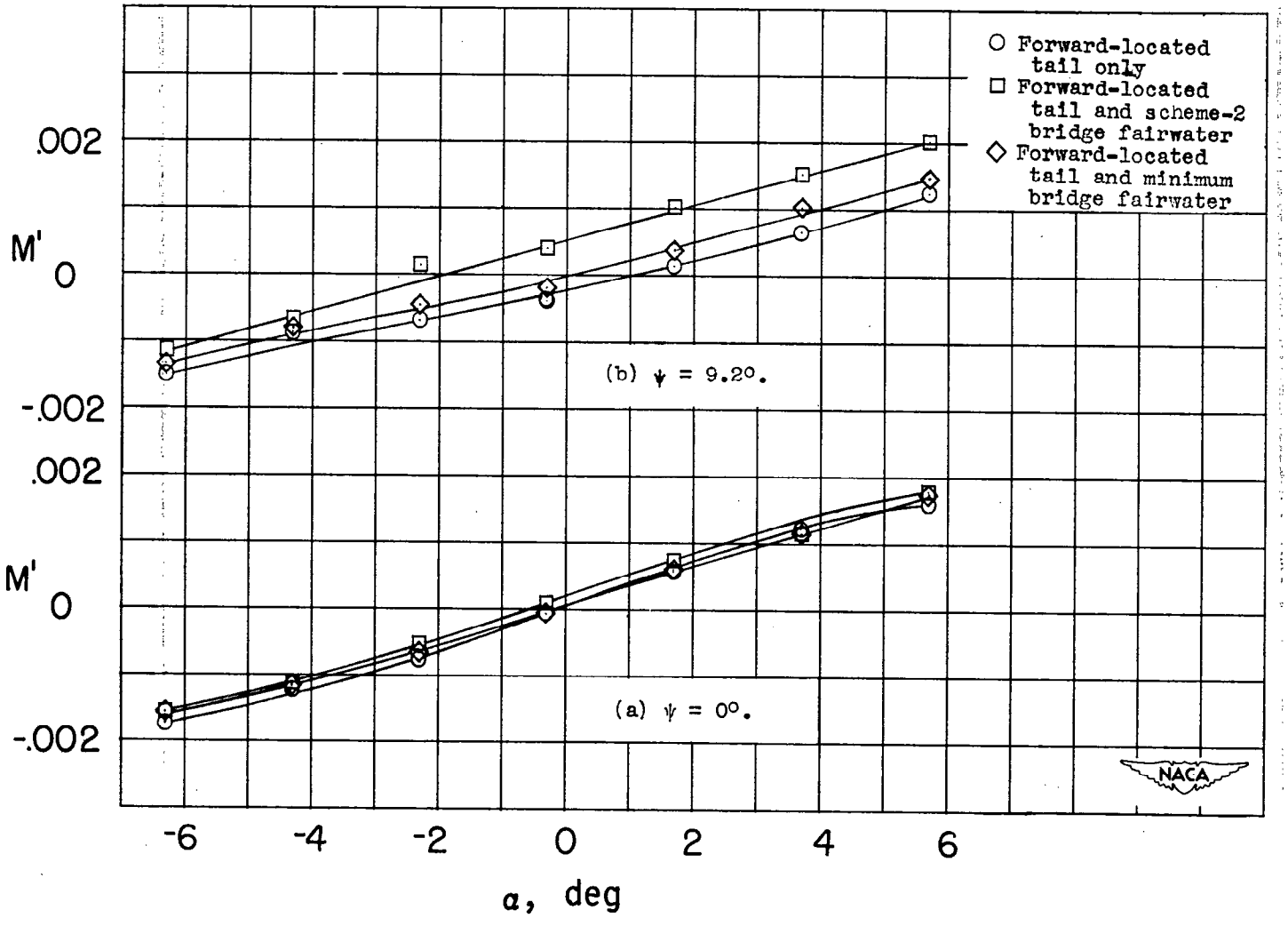

Figure 13.- Variation of pitching-moment coefficient with angle of attack for the model with and without bridge fairwater. Forward-located tails installed; $\delta_r = 0^\circ$; $\delta_s = 0^\circ$.

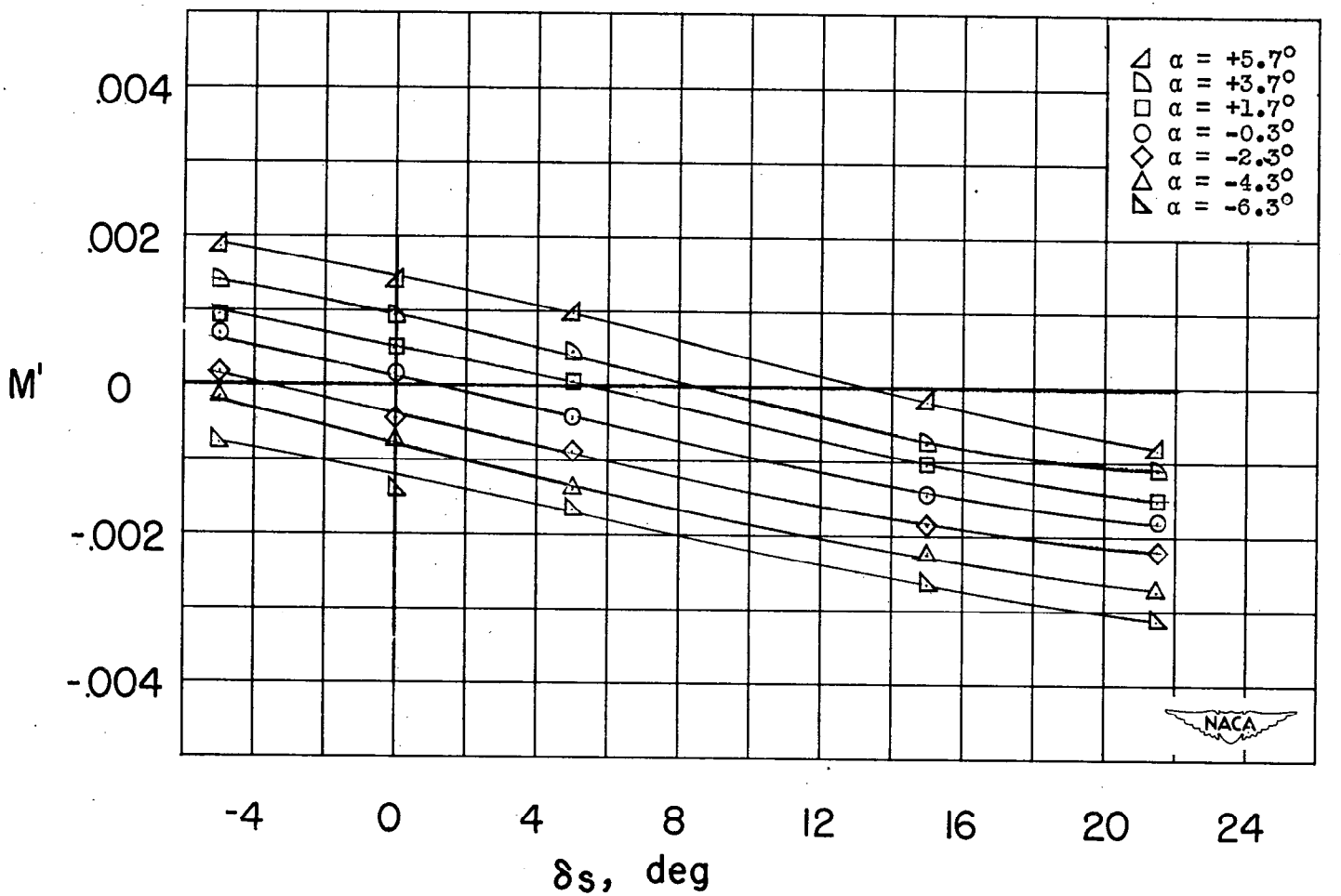

(a) Scheme-2 tail with large horizontal surfaces.

Figure 14.- Variation of pitching-moment coefficient with diving-plane deflection and angle of attack for three tail configurations. $\psi = 0^{\circ}$; $\delta_r = 0^{\circ}$.

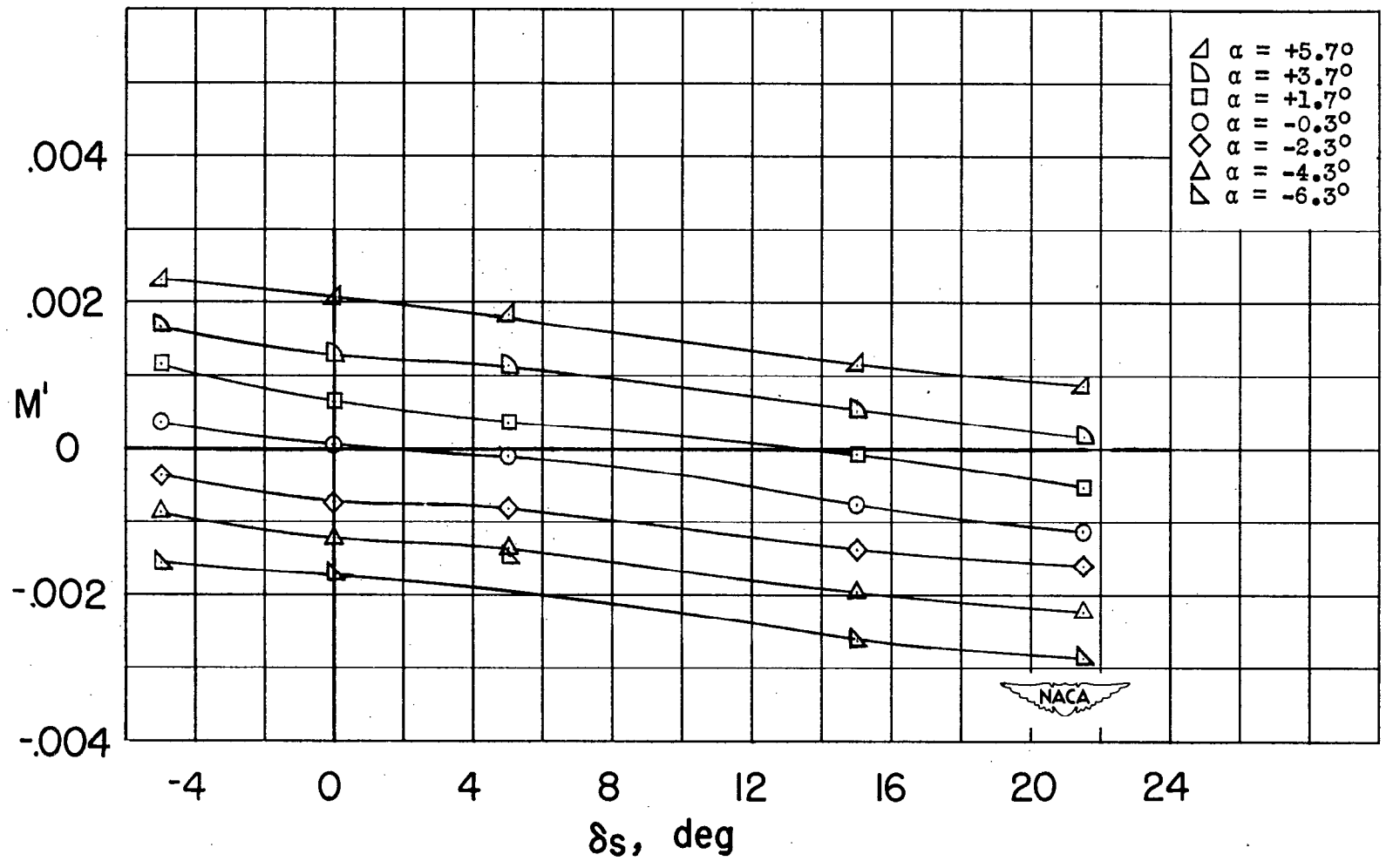

CONFIDENTIAL

(b) Scheme-2 tail with small horizontal surfaces.

Figure 14.- Continued.

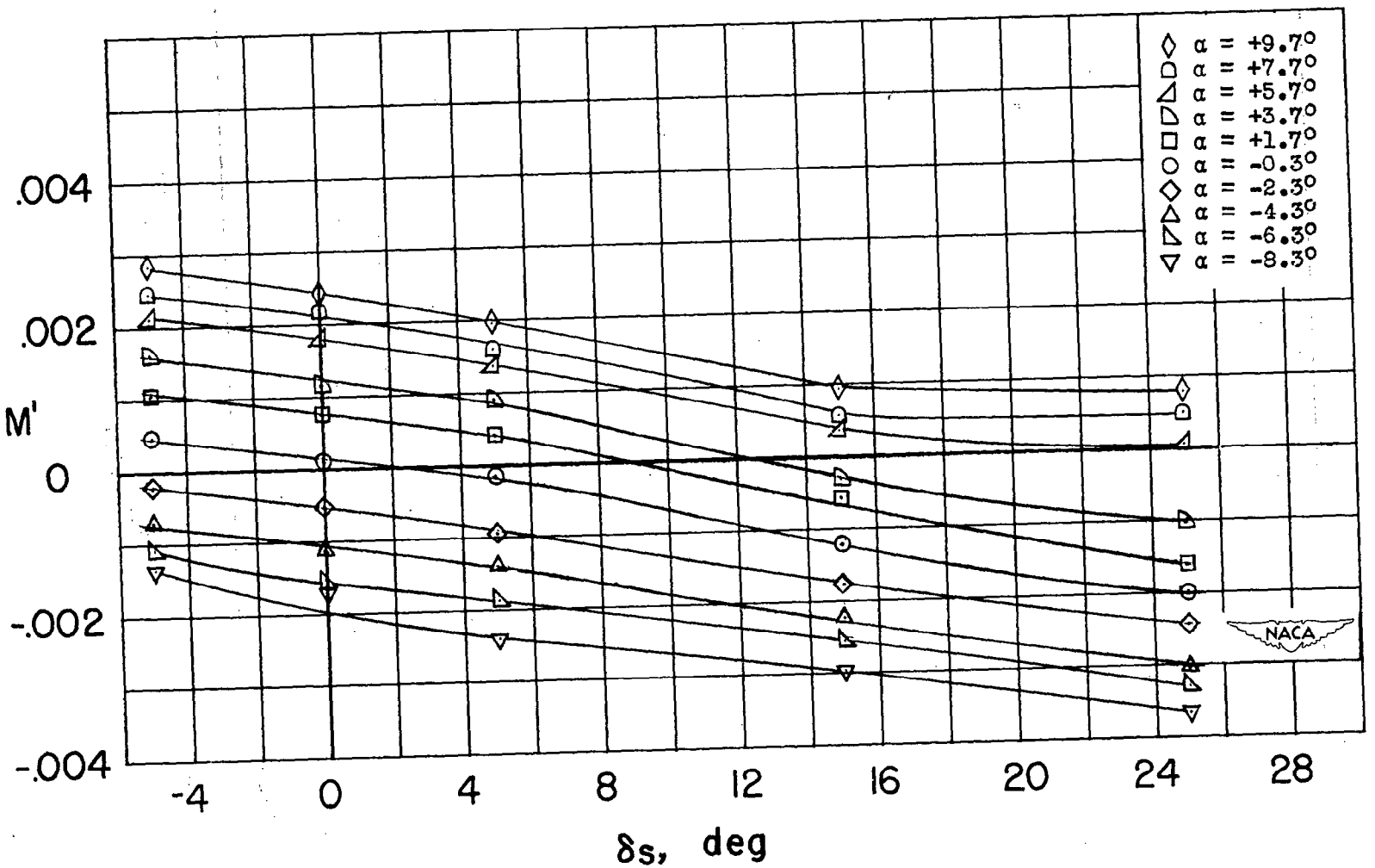

(c) Forward-located tails.

Figure 14.- Concluded.

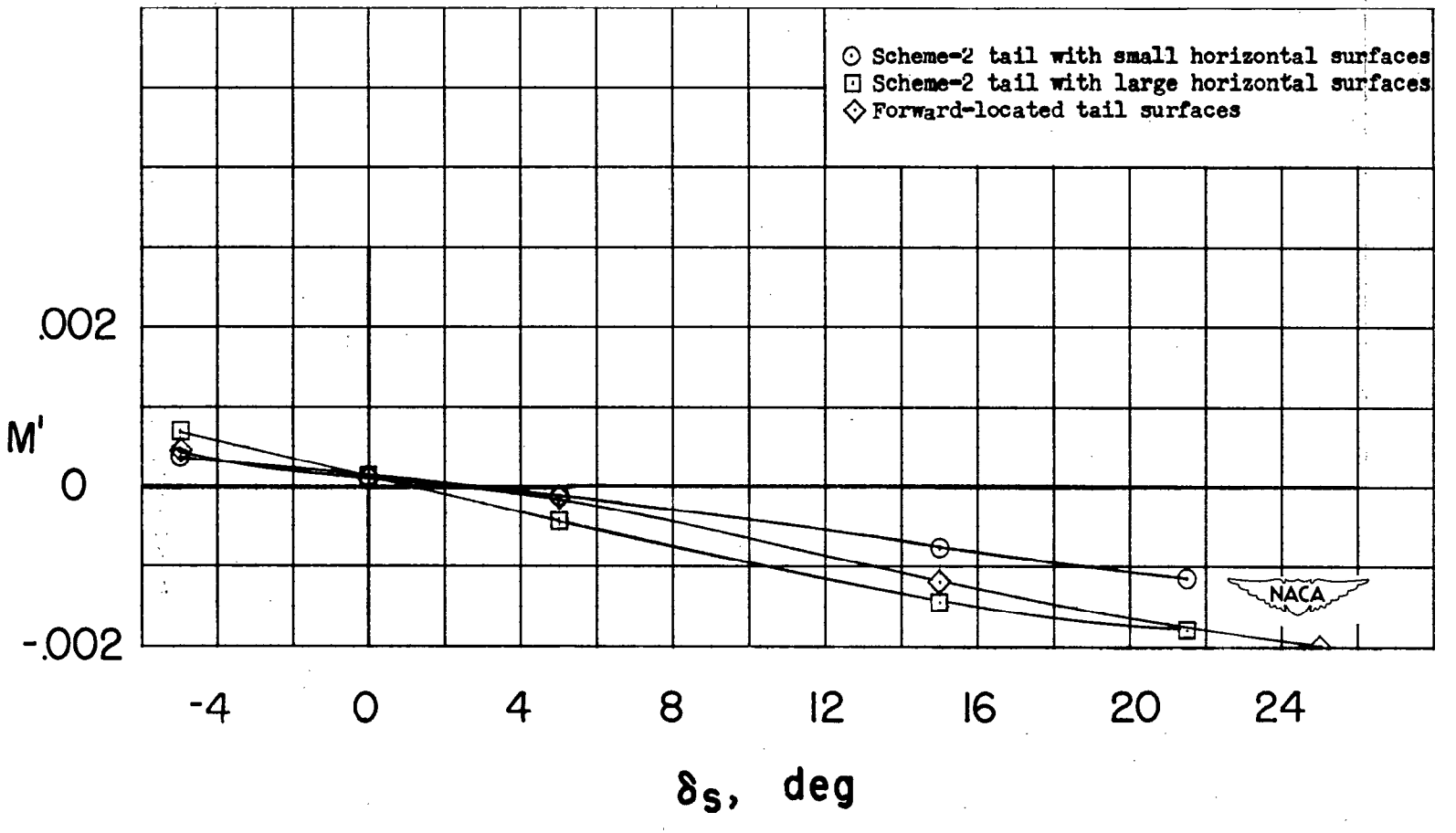

Figure 15.- Pitching-moment-coefficient variation with diving-plane deflection for three tail configurations. $\alpha = -0.3^{\circ}$; $\psi = 0^{\circ}$; $\delta_r = 0^{\circ}$.

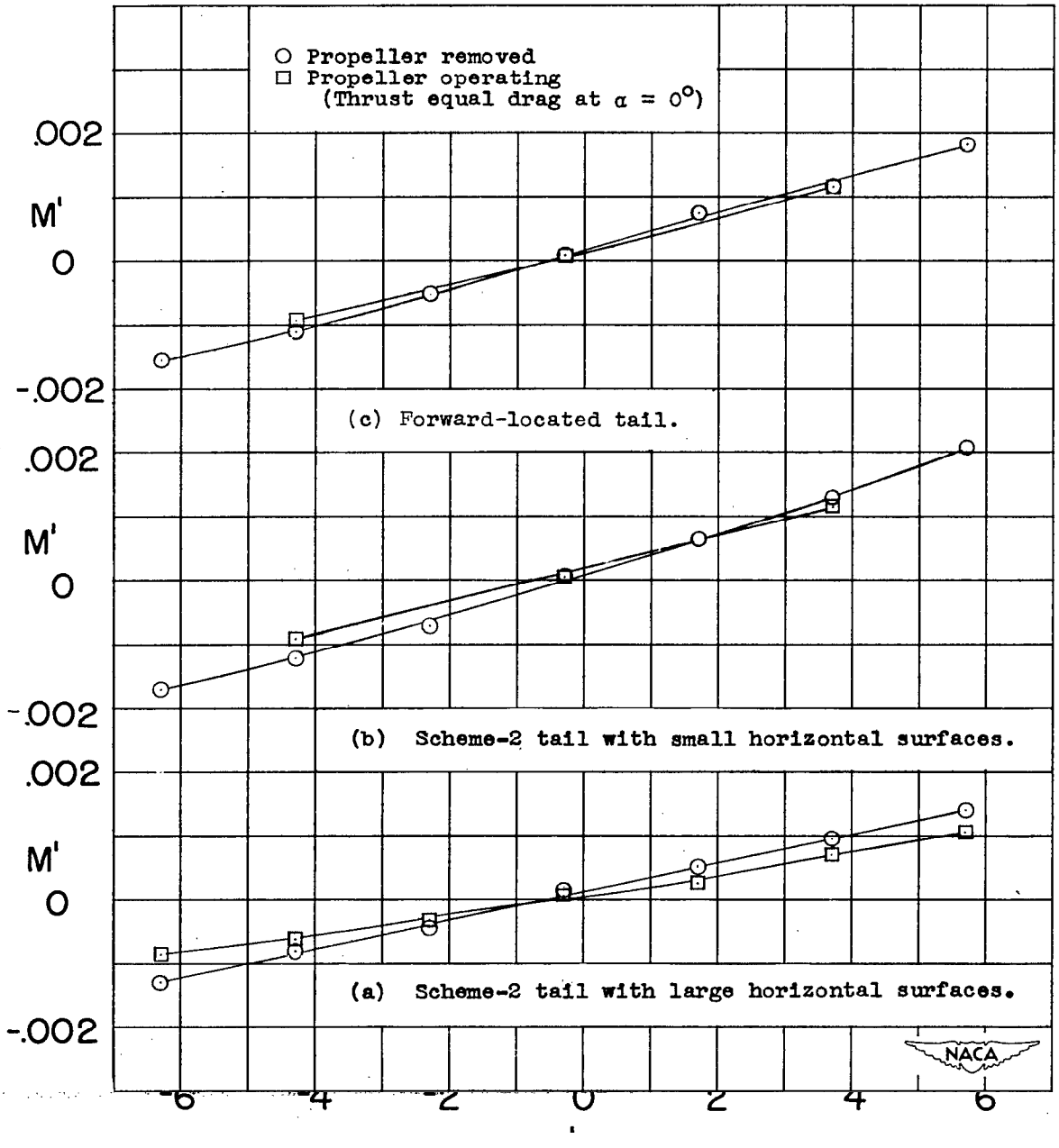
○ Propeller removed
□ Propeller operating
(Thrust equal drag at α = 0°)
.002
M'
0
-.002
(c) Forward-located tail.
.002
M'
0
-.002
(b) Scheme-2 tail with small horizontal surfaces.
.002
M'
0
-.002
(a) Scheme-2 tail with large horizontal surfaces.
NACA
-6
-4
-2
0
2
4
6

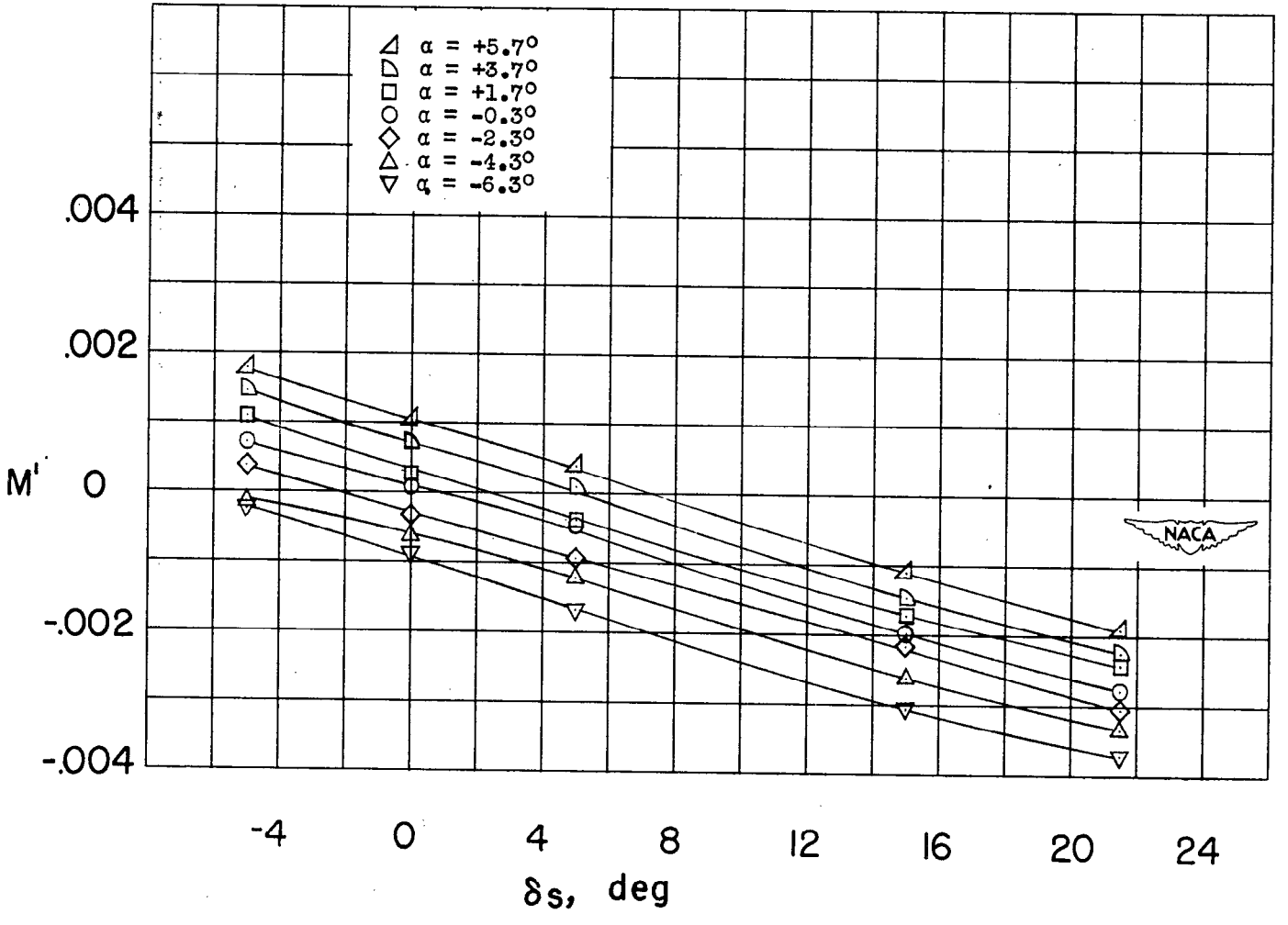

Figure 17.- Variation of pitching-moment coefficient with diving-plane deflection and angle of attack for scheme-2 tail with propeller operating. Large horizontal tail surfaces and scheme-2 bridge fairwater installed. $\psi = 0^{\circ}$; $\delta_r = 0^{\circ}$.

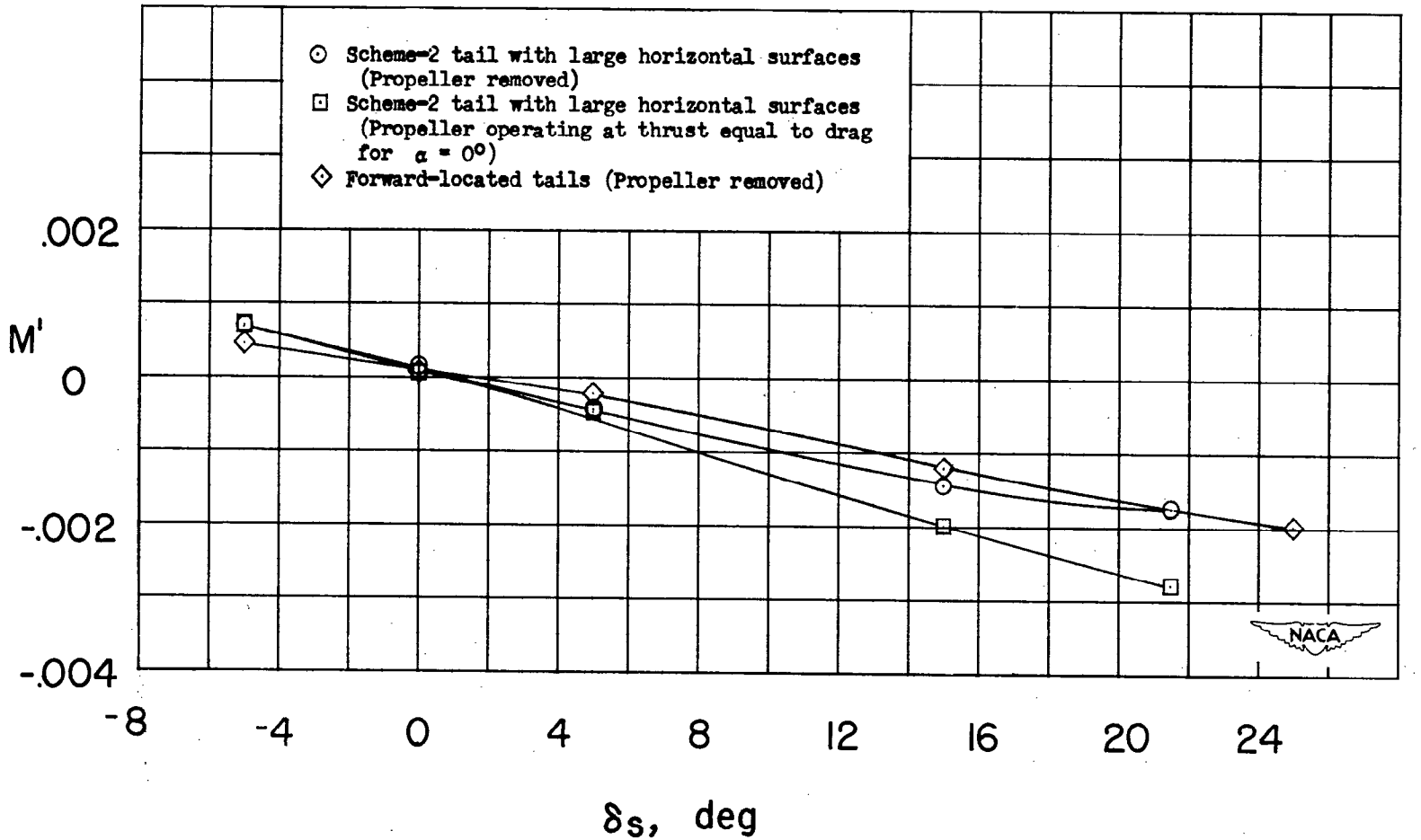

Figure 18.- Variation of pitching-moment coefficient with diving-plane deflection for two tail configurations with and without propeller operation. $\psi = 0^{\circ}$; $\alpha = 0^{\circ}$; $\delta_r = 0^{\circ}$.

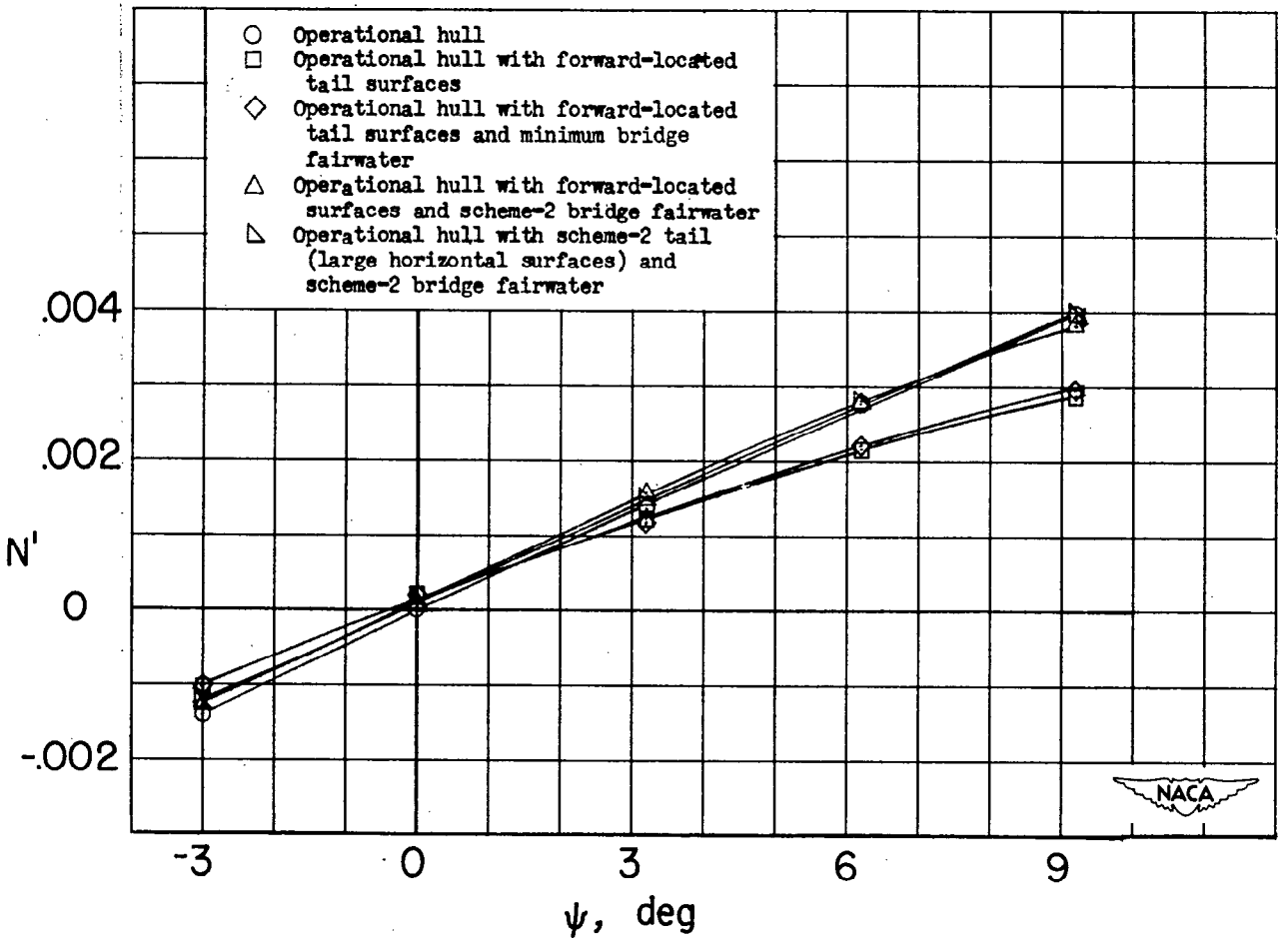

(a) Yawing-moment coefficient, N'.

Figure 19.- Variation of yawing-moment coefficient, rolling-moment coefficient, pitching-moment coefficient, and lateral-force coefficient with angle of yaw for five model configurations. $\alpha = 0.3^{\circ}$; $\delta_r = 0^{\circ}$; $\delta_s = 0^{\circ}$.

CONFIDENTIAL

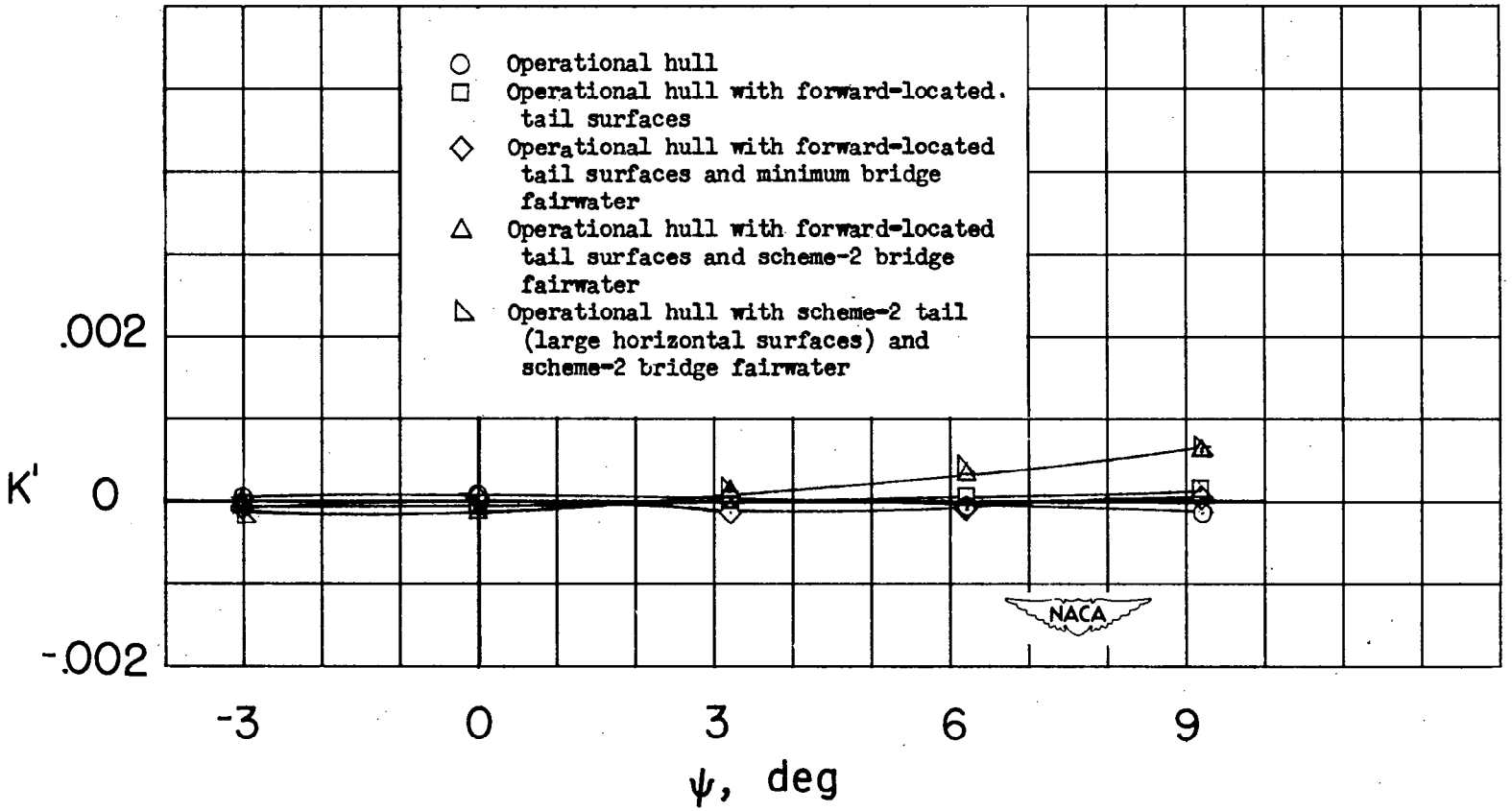

CONFIDENTIAL

(b) Rolling-moment coefficient, K'.

Figure 19.- Continued.

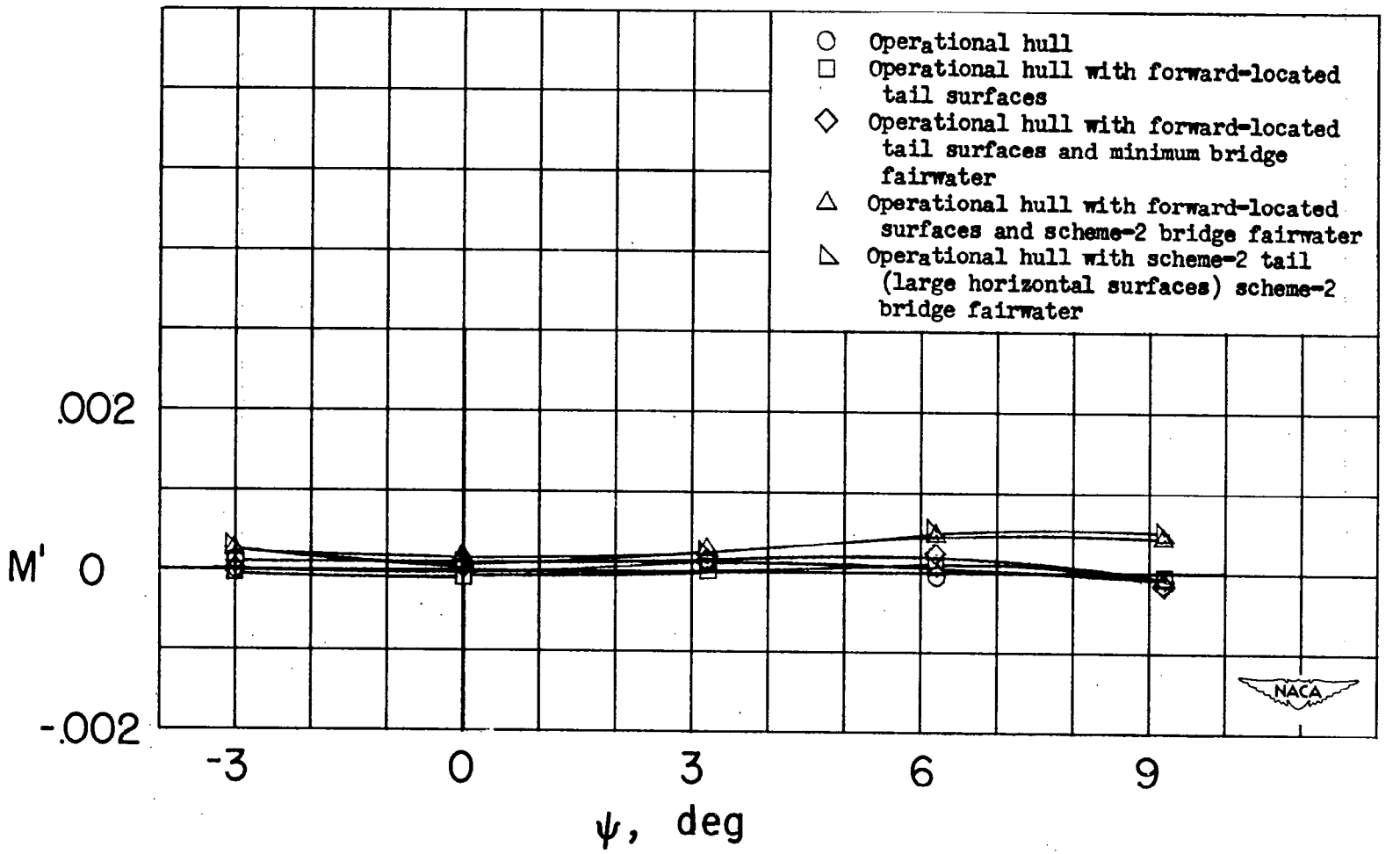

(c) Pitching-moment coefficient, M'.

Figure 19.- Continued.

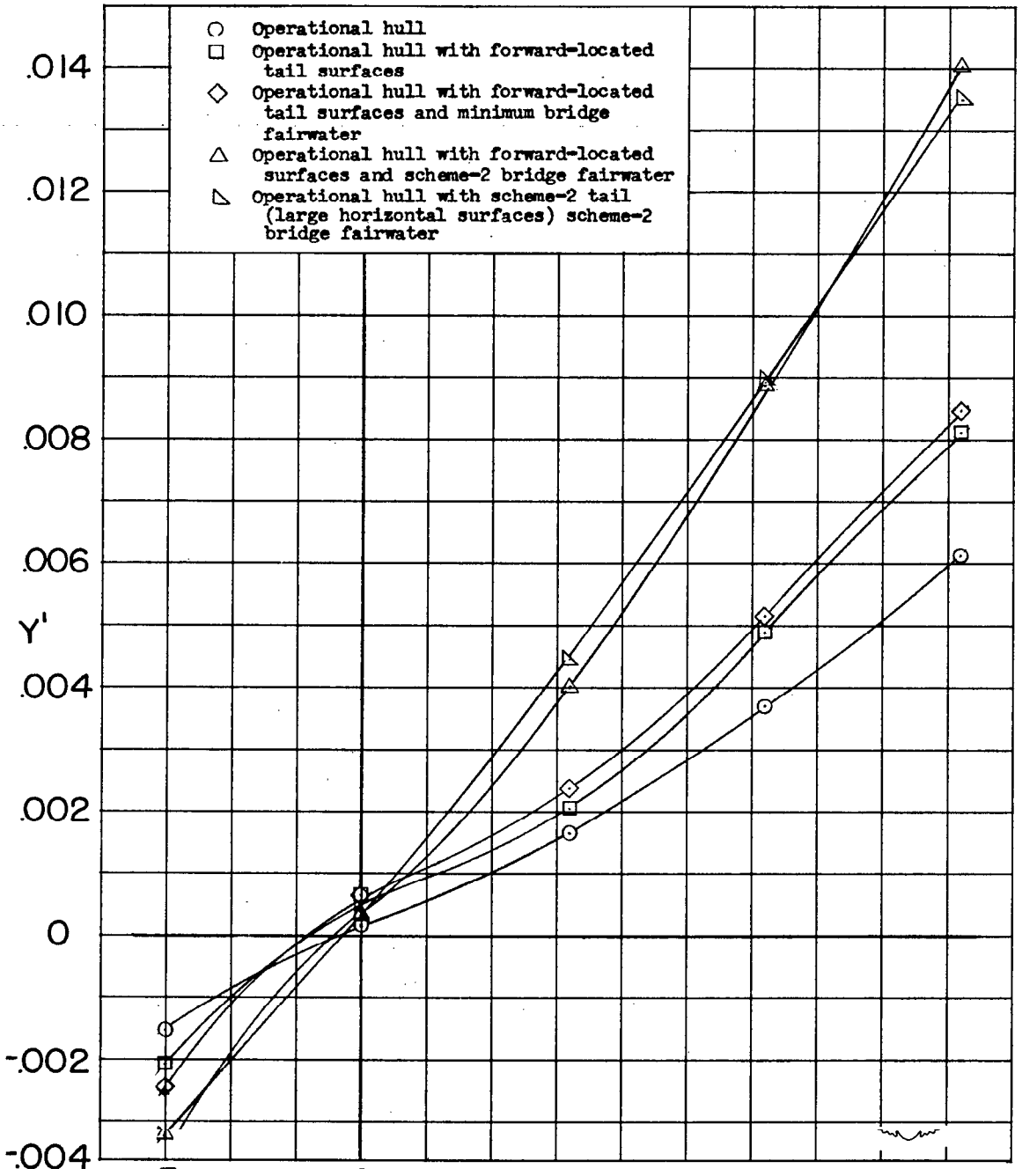
Operational hull
Operational hull with forward-located tail surfaces
Operational hull with forward-located tail surfaces and minimum bridge fairwater
Operational hull with forward-located surfaces and scheme-2 bridge fairwater
Operational hull with scheme-2 tail (large horizontal surfaces) scheme-2 bridge fairwater
.014
.012
.010
.008
.006
Y'
.004
.002
0
-.002
-.004

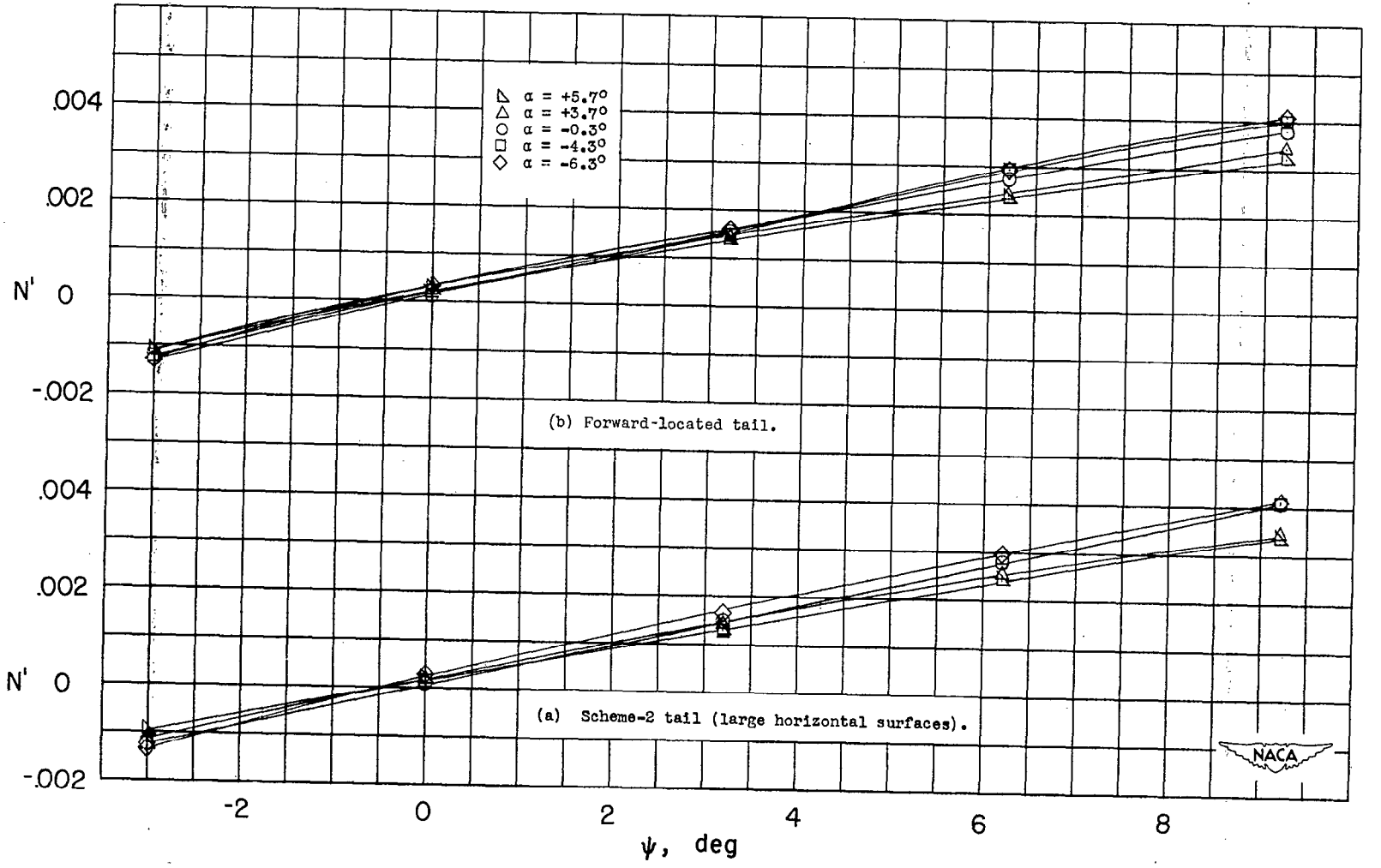

Figure 20.- Variation of yawing-moment coefficient with angle of yaw and angle of attack with scheme-2 bridge fairwater installed. $\delta_r = 0^o$; $\delta_s = 0^o$.

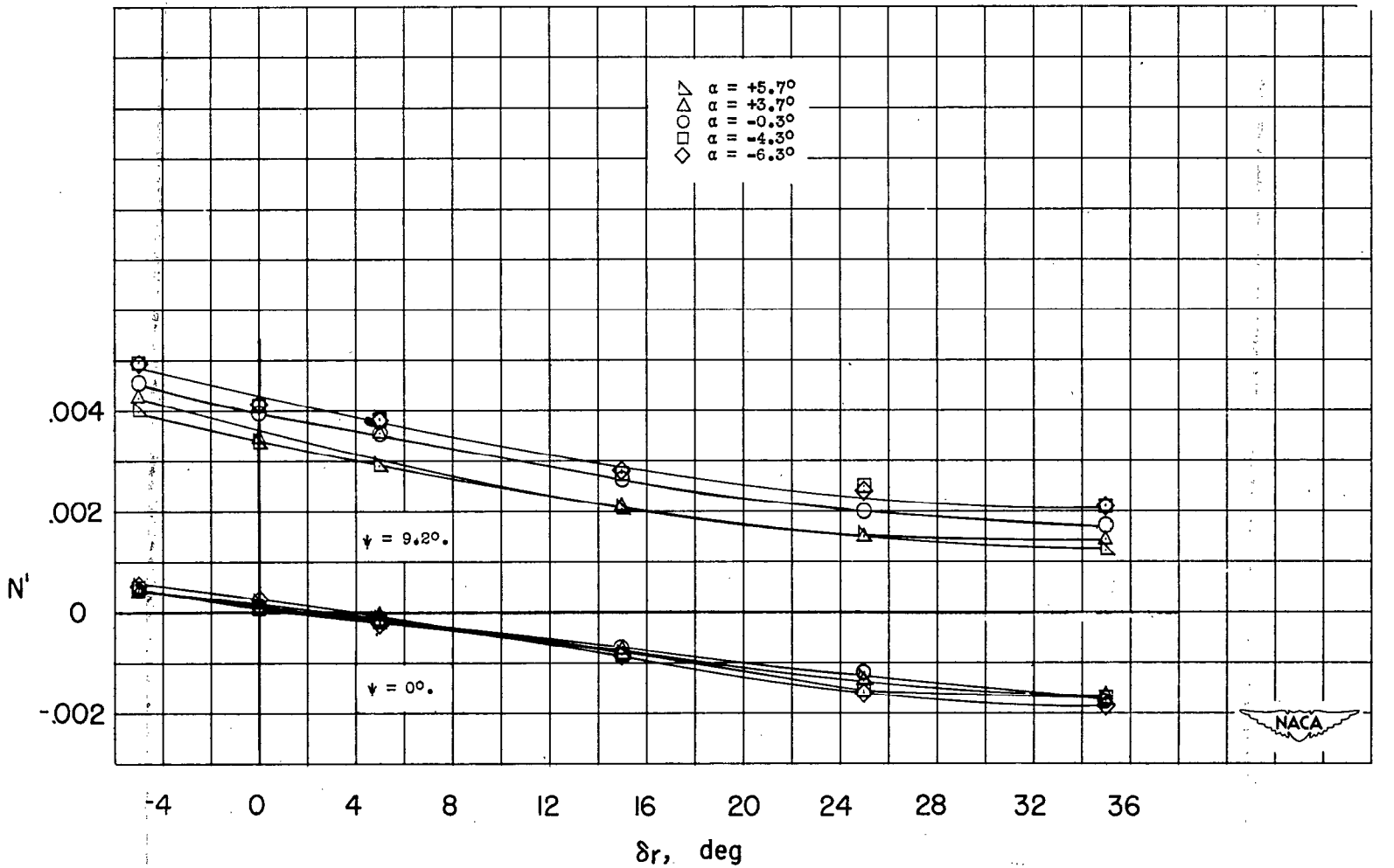

(a) Complete model with scheme-2 tail; $\delta_s = 0^\circ$.

Figure 21.- Variation of yawing-moment coefficient with rudder deflection at different model attitudes.

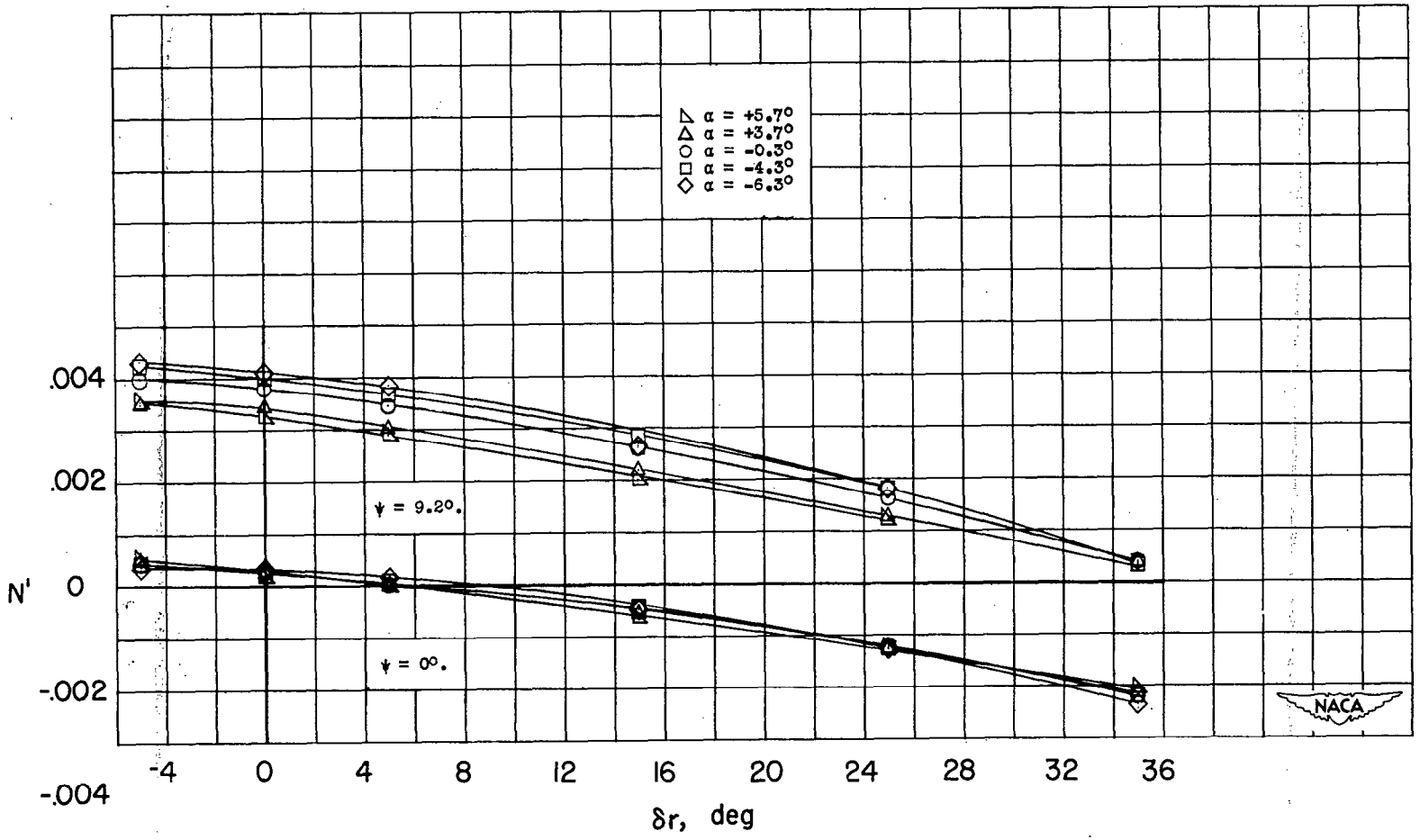

(b) Complete model with forward-located tail; $\delta_s = 0^\circ$.

Figure 21.- Concluded.

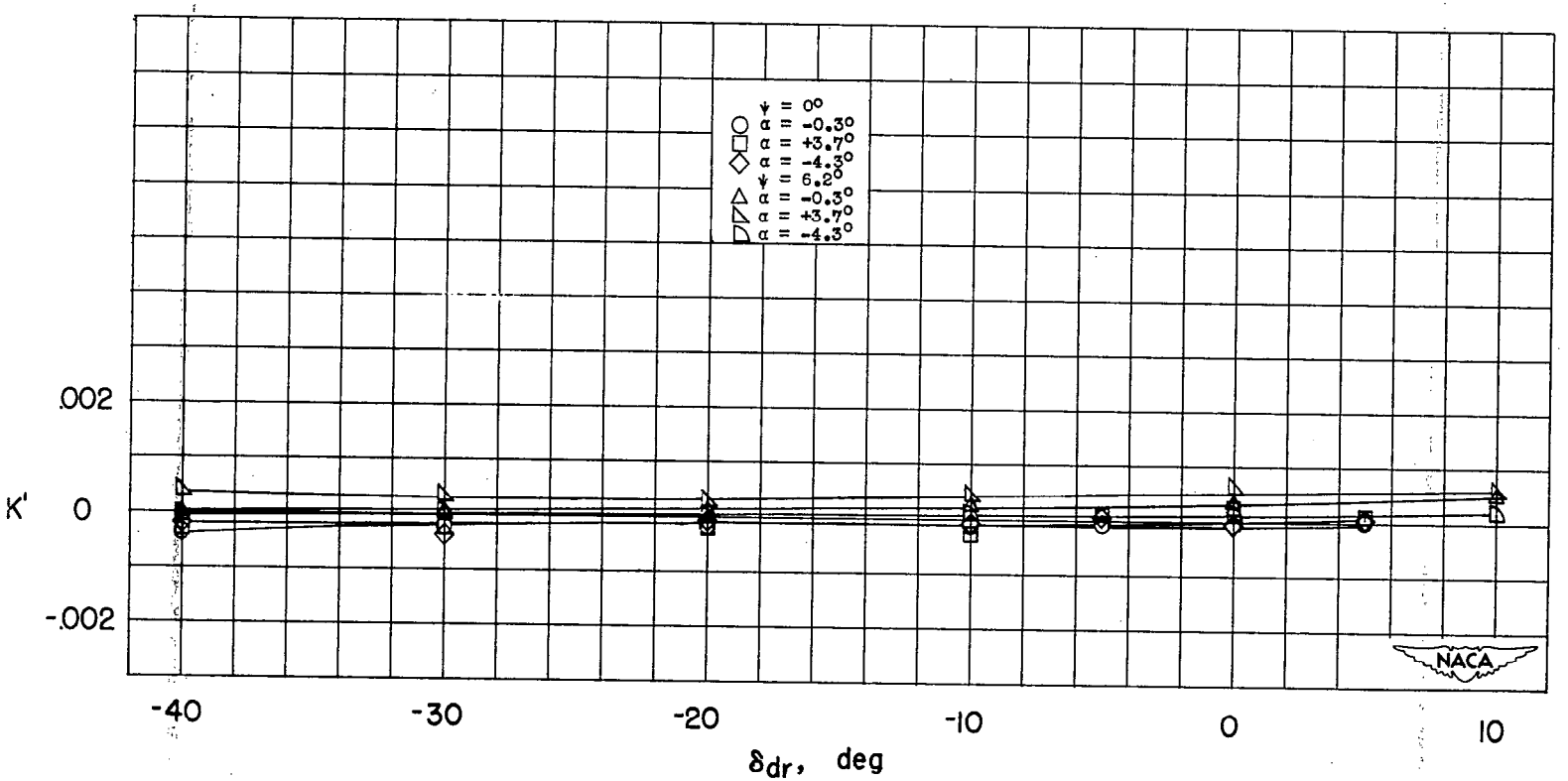

(a) Rolling-moment coefficient, K'.

Figure 22.- Variation of rolling-moment coefficient, yawing-moment coefficient, pitching-moment coefficient, and lateral-force coefficient with deflection of bridge-fairwater dorsal rudder.

CONFIDENTIAL

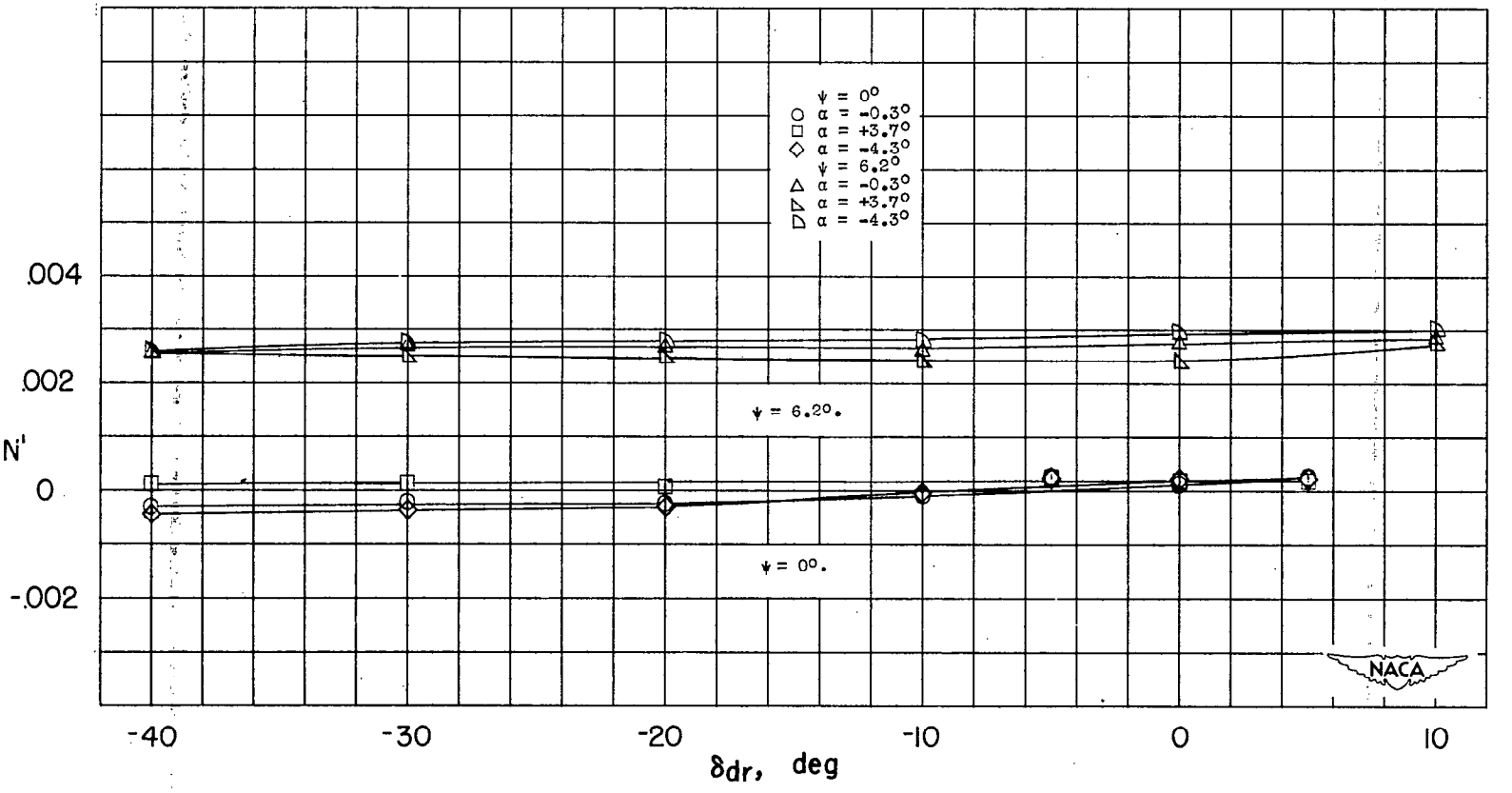

(b) Yawing-moment coefficient, N'.

Figure 22.- Continued.

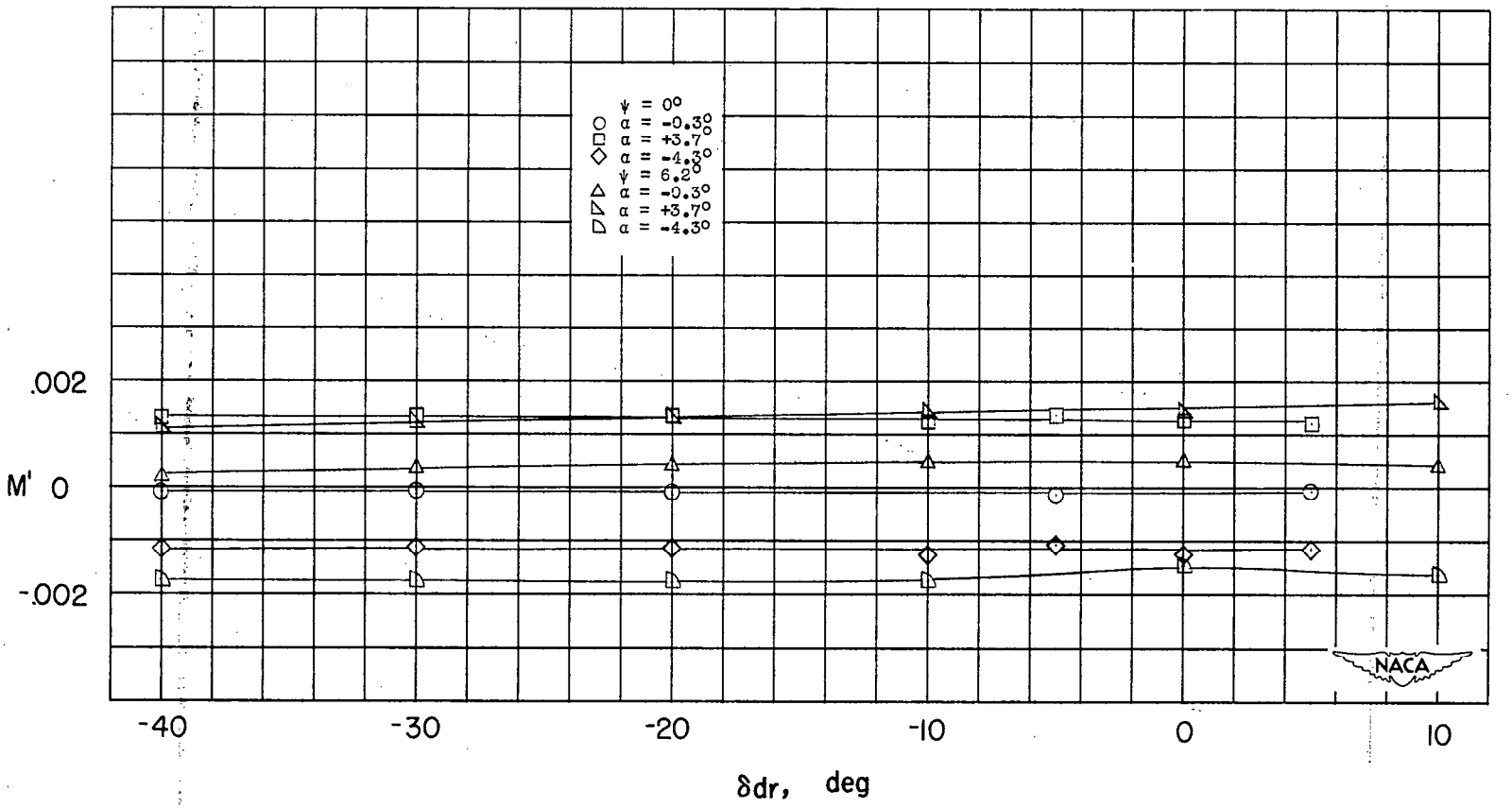

(c) Pitching-moment coefficient, M'.

Figure 22.- Continued.

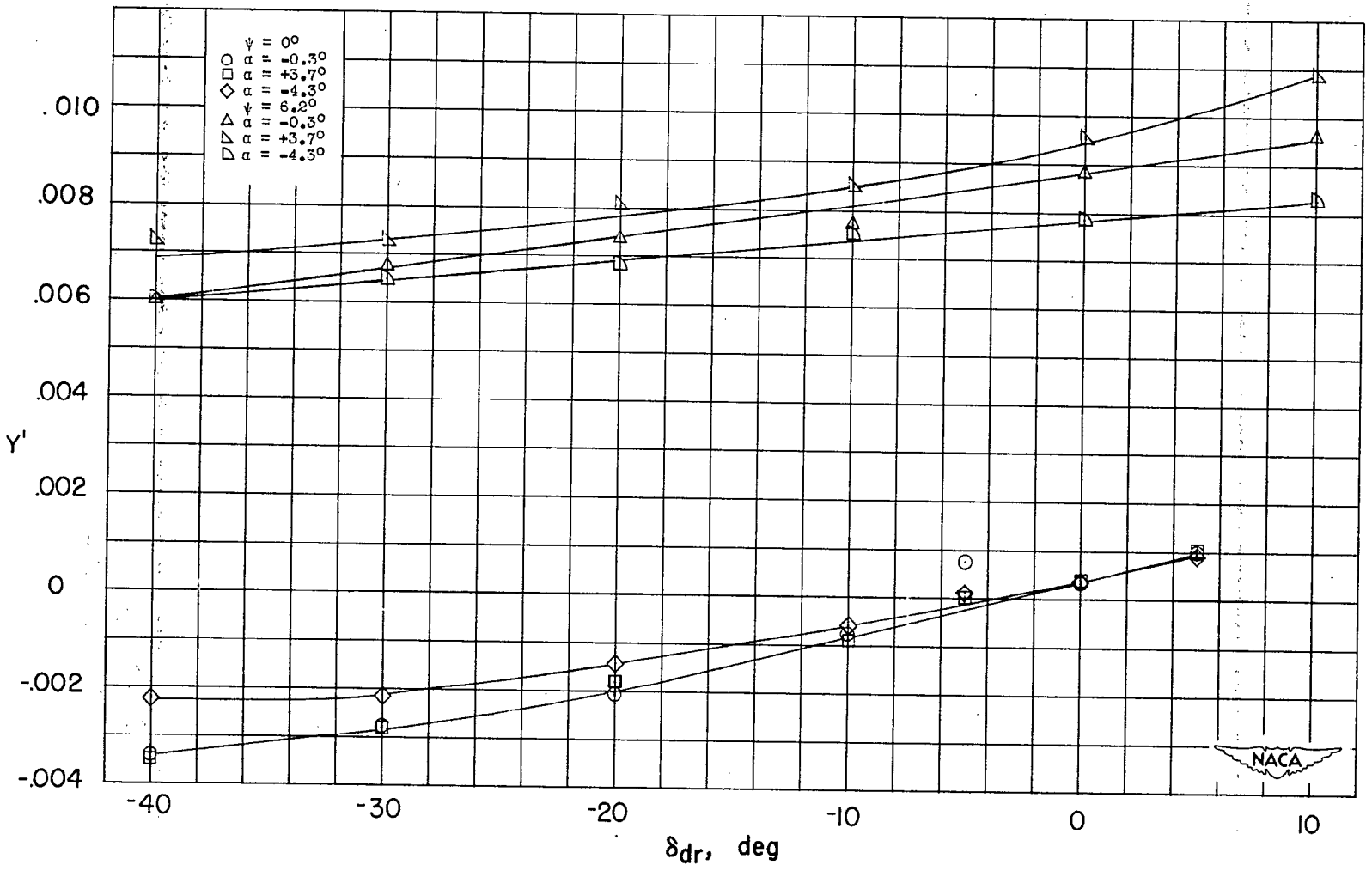

(d) Lateral-force coefficient, Y'.

Figure 22.- Concluded.

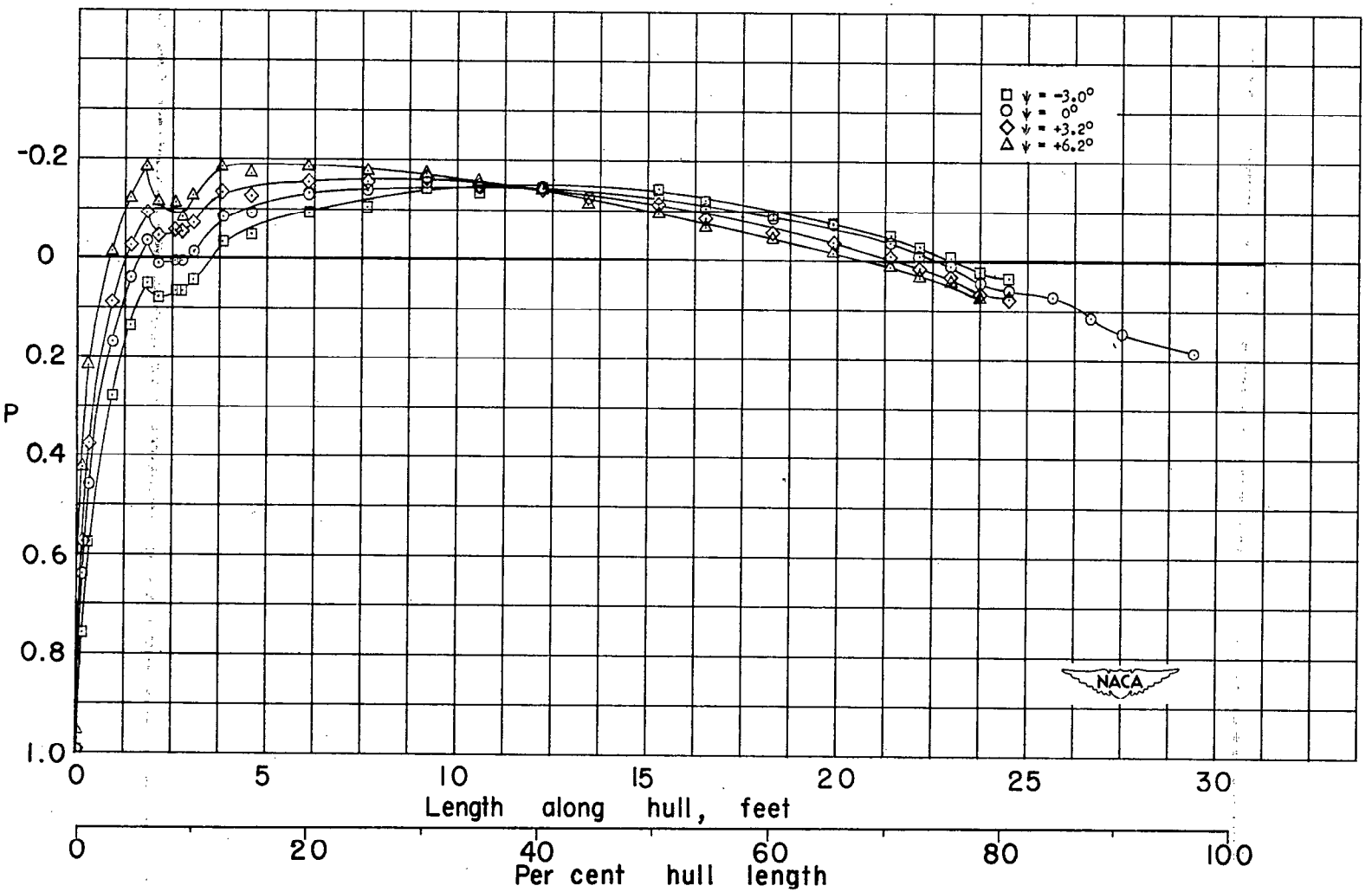

Figure 23.- Effect of angle of yaw on hull pressure distribution along the starboard side of hull. $\alpha = -0.3^{\circ}$.

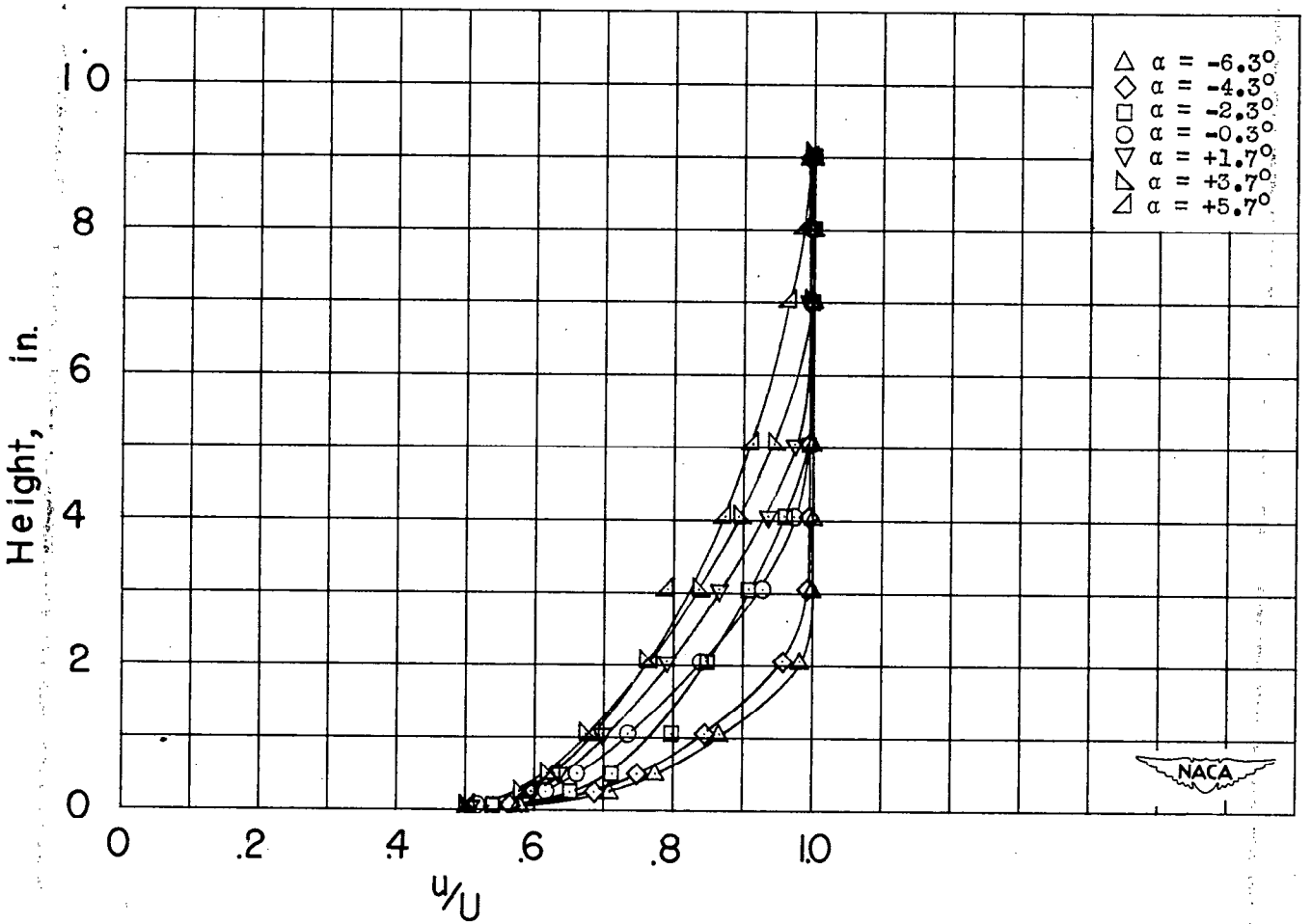

(a) Position 0.80l.

Figure 24.- Effect of angle of attack on velocity distribution in the boundary layer along top center line of basic hull. Bridge fairwater removed.

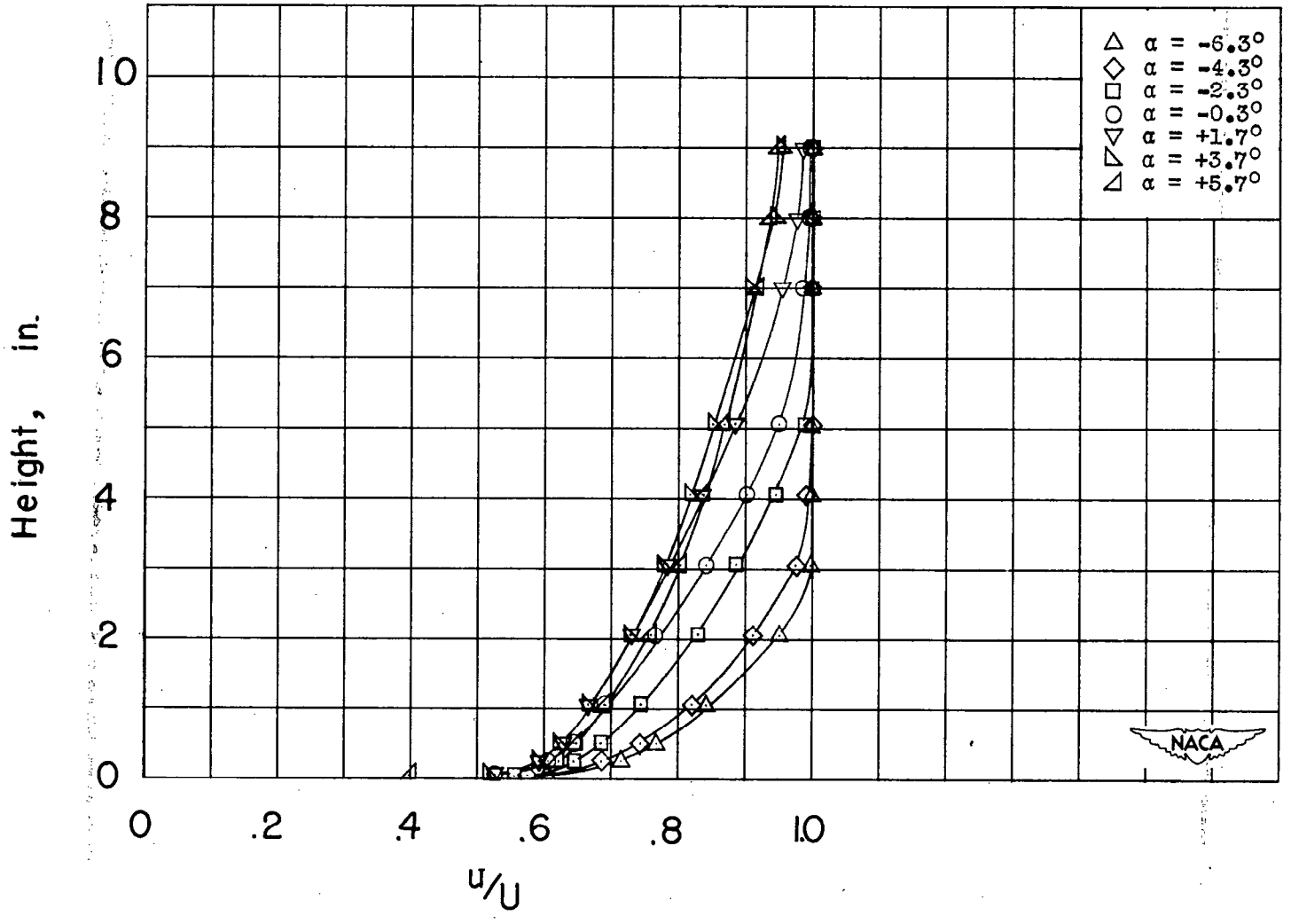

(b) Position 0.88ℓ.

Figure 24.- Continued.

CONFIDENTIAL

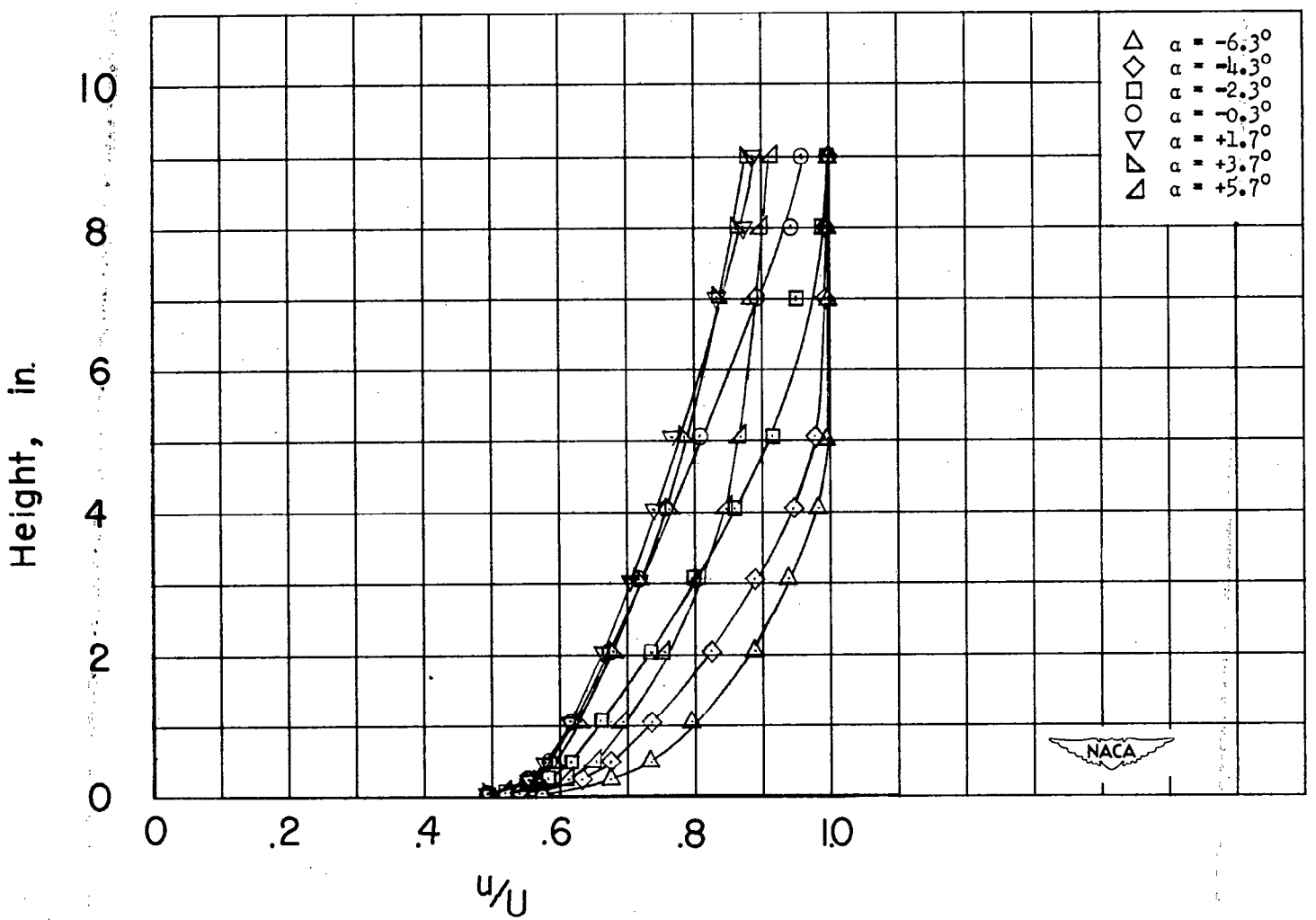

(c) Position 0.96ℓ.

Figure 24.- Concluded.

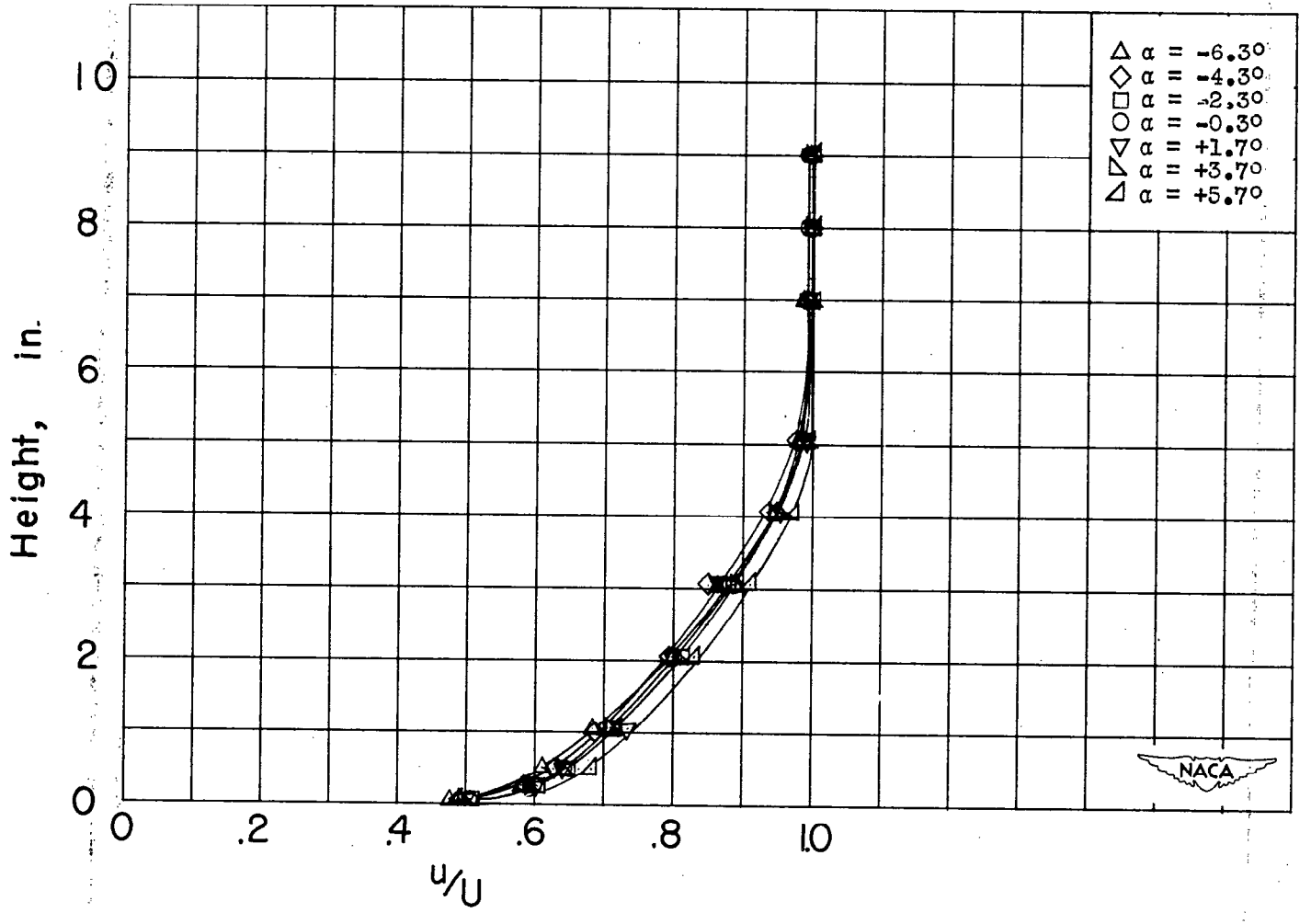

(a) Position 0.80ℓ.

Figure 25.- Effect of angle of attack on velocity distribution in the boundary layer along starboard side center line of basic hull.

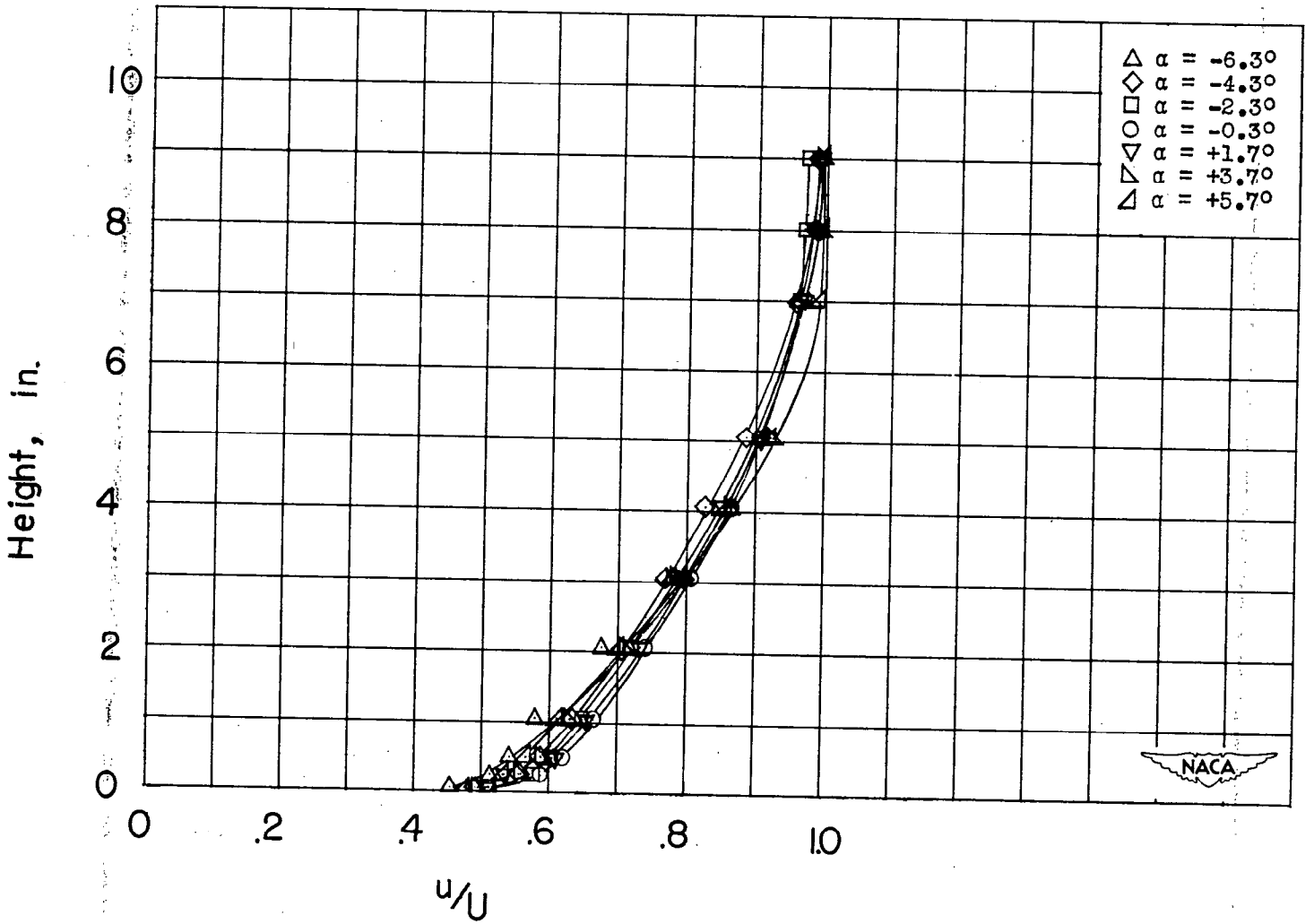

(b) Position 0.88ℓ.

Figure 25.- Continued.

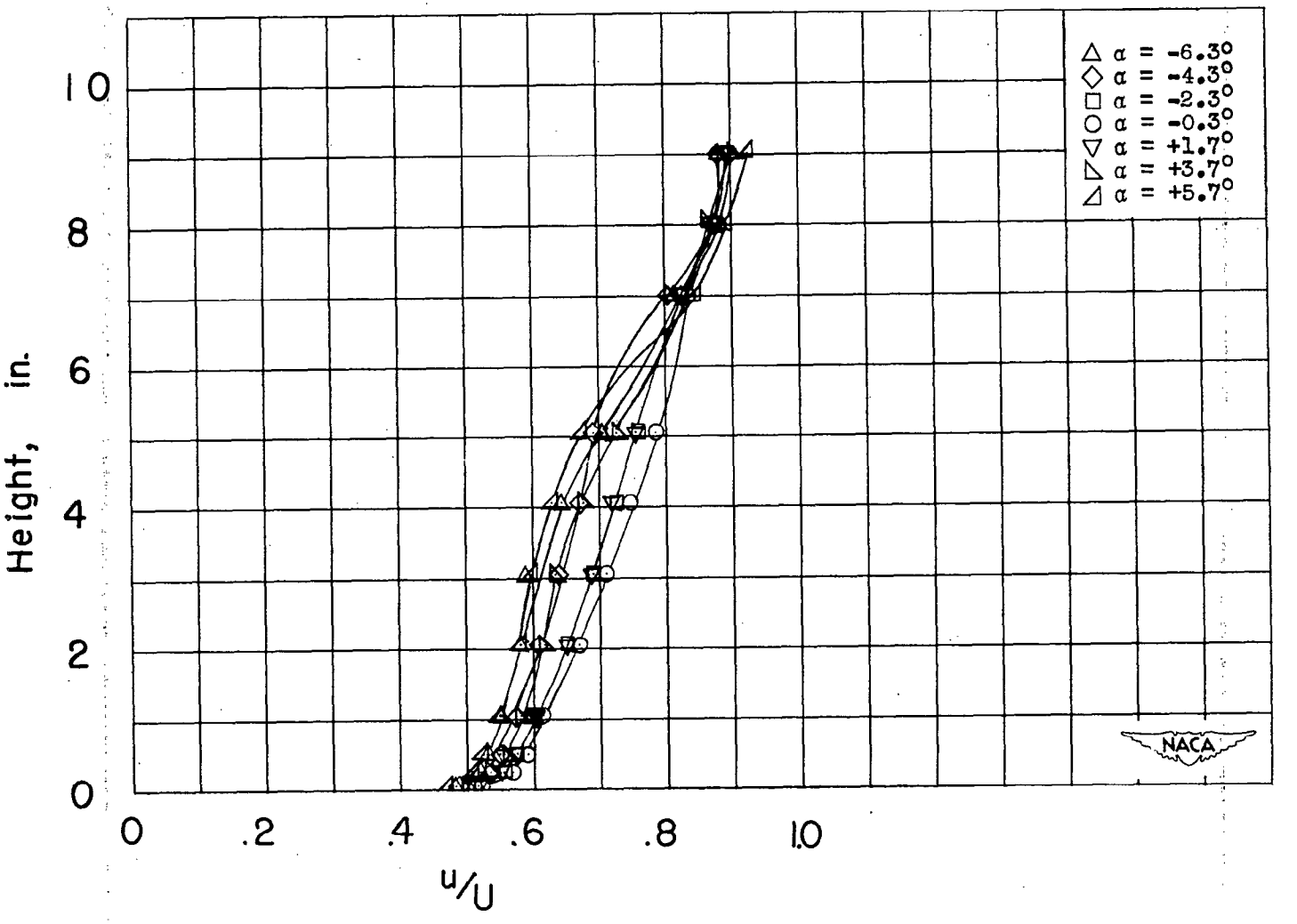

(c) Position 0.96l.

Figure 25.- Concluded.

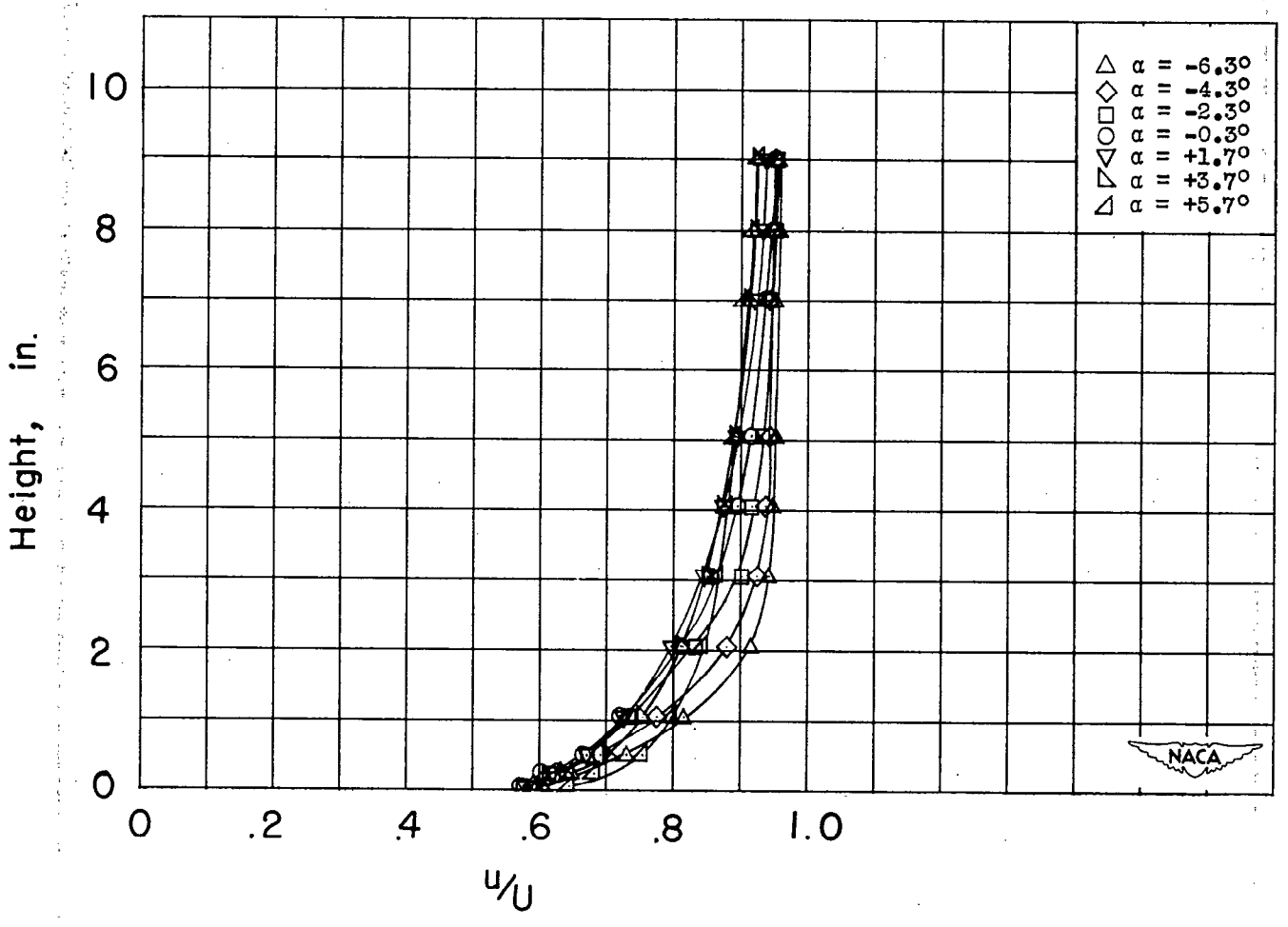

(a) Position 0.88ℓ.

Figure 26.- Effect of angle of attack on velocity distribution in the boundary layer along top center line of operational hull. Scheme-2 bridge fairwater installed.

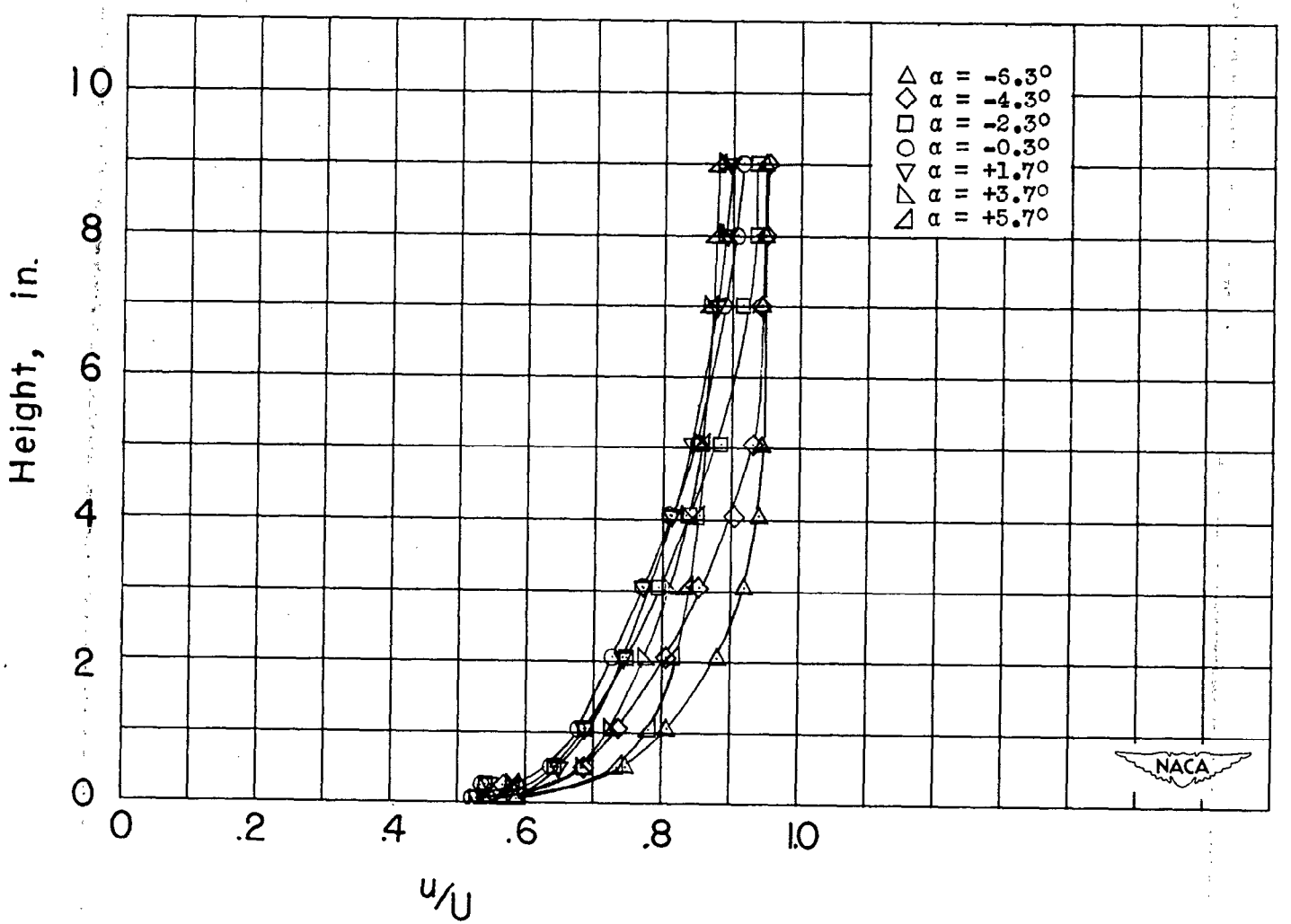

(b) Position 0.96l.

Figure 26.- Concluded.

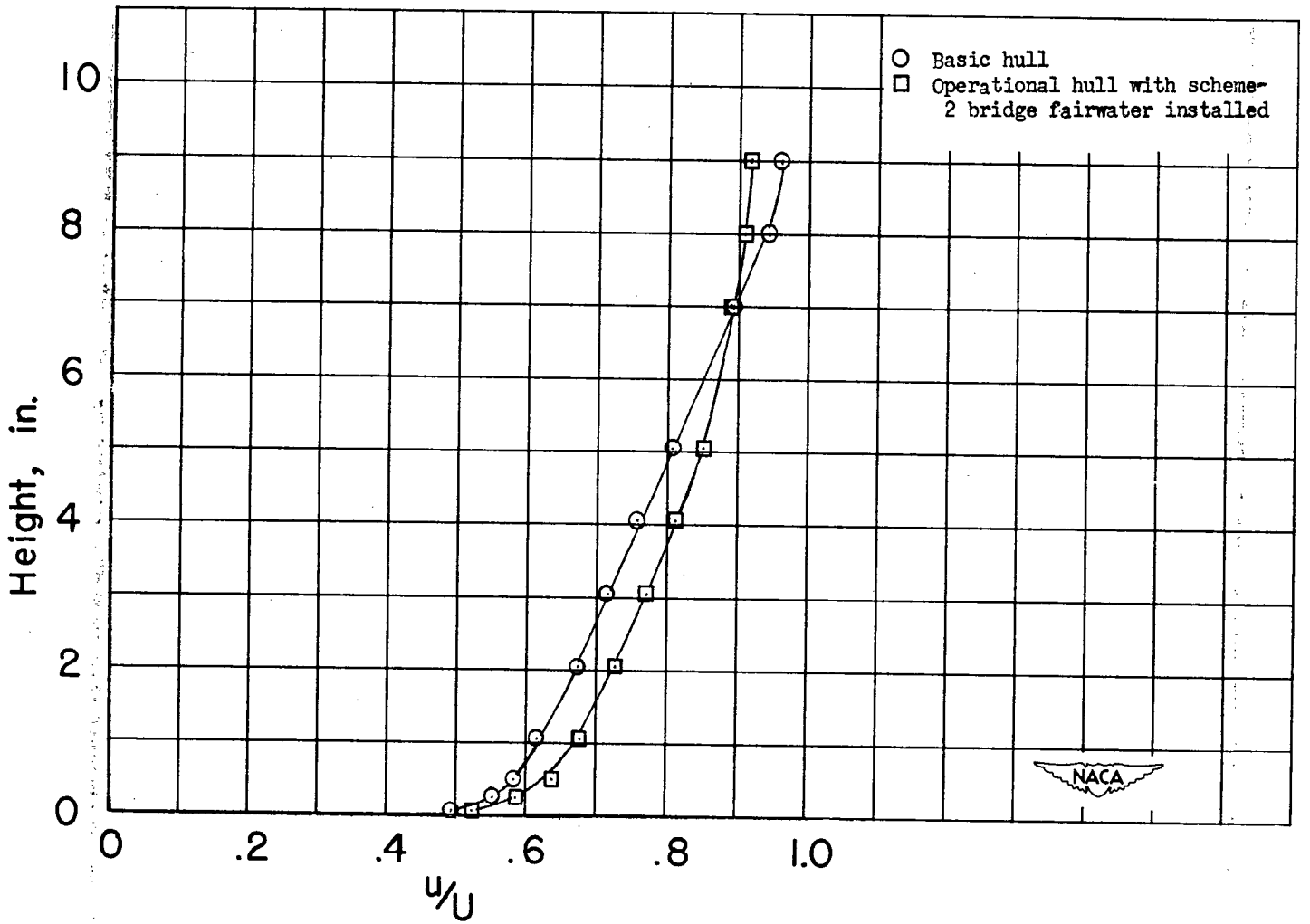

Figure 27.- Effect of hull condition on velocity profiles in the boundary layer along the top center line of the hull. $\alpha = -0.3^{\circ}$; $\psi = 0^{\circ}$; Position, 0.96l.

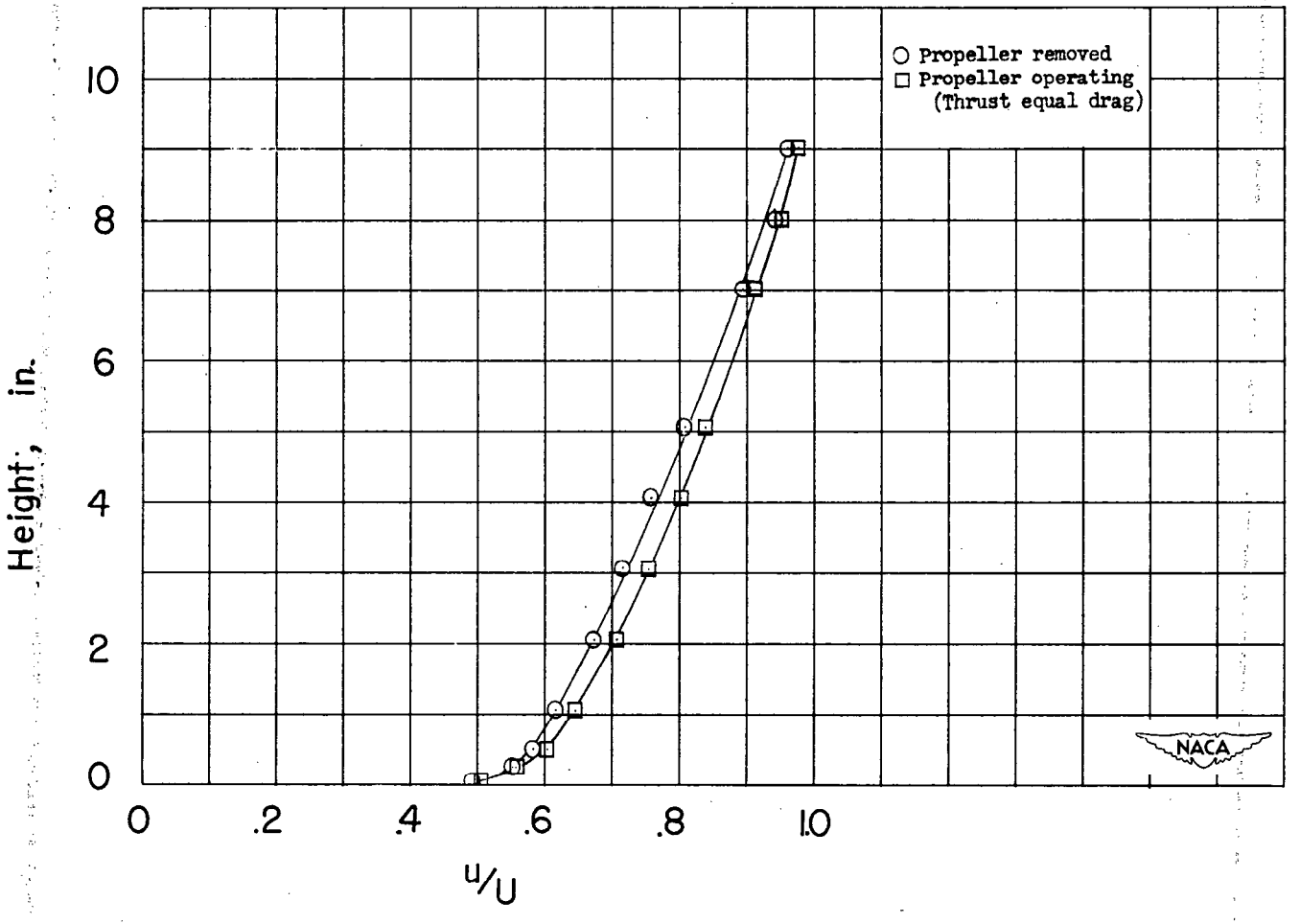

(a) Top center line.

Figure 28.- Effect of propeller operation on velocity distribution in the boundary layer at longitudinal station 0.96l. Basic hull; $\alpha = 0^{\circ}$; $\psi = 0^{\circ}$.

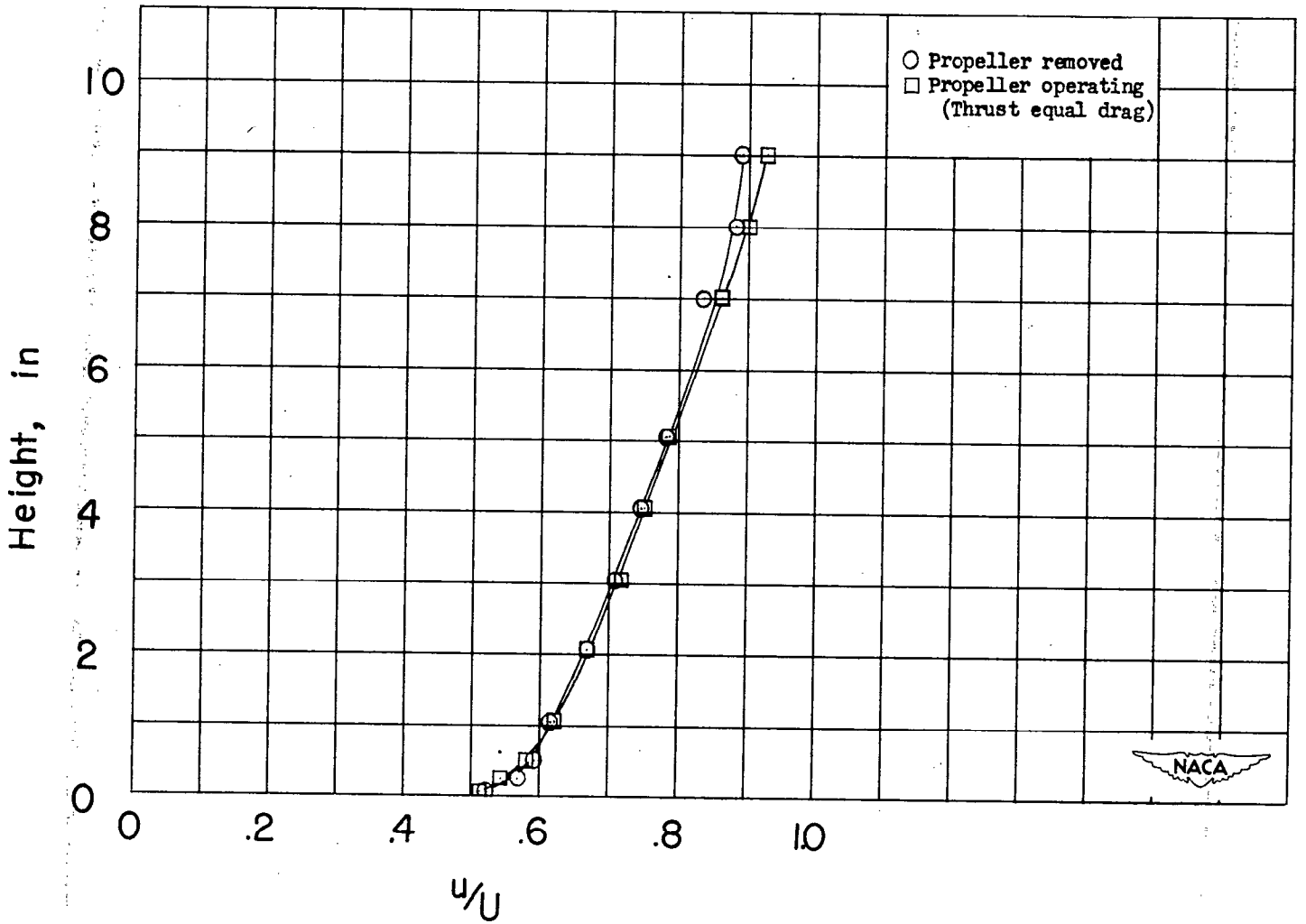

(b) Side center line.

Figure 28.- Concluded.

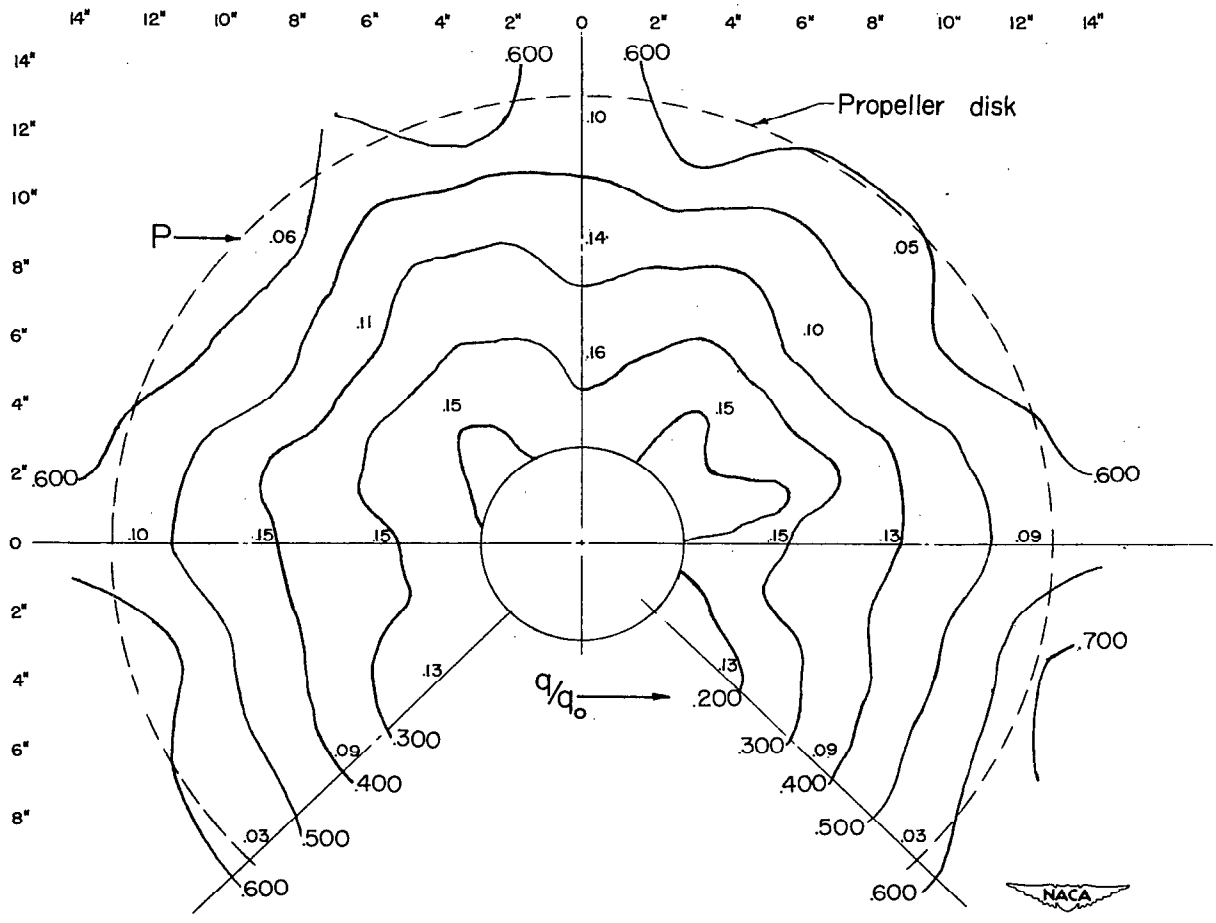

Figure 20. Variation of local dynamic pressure ratios in the region of

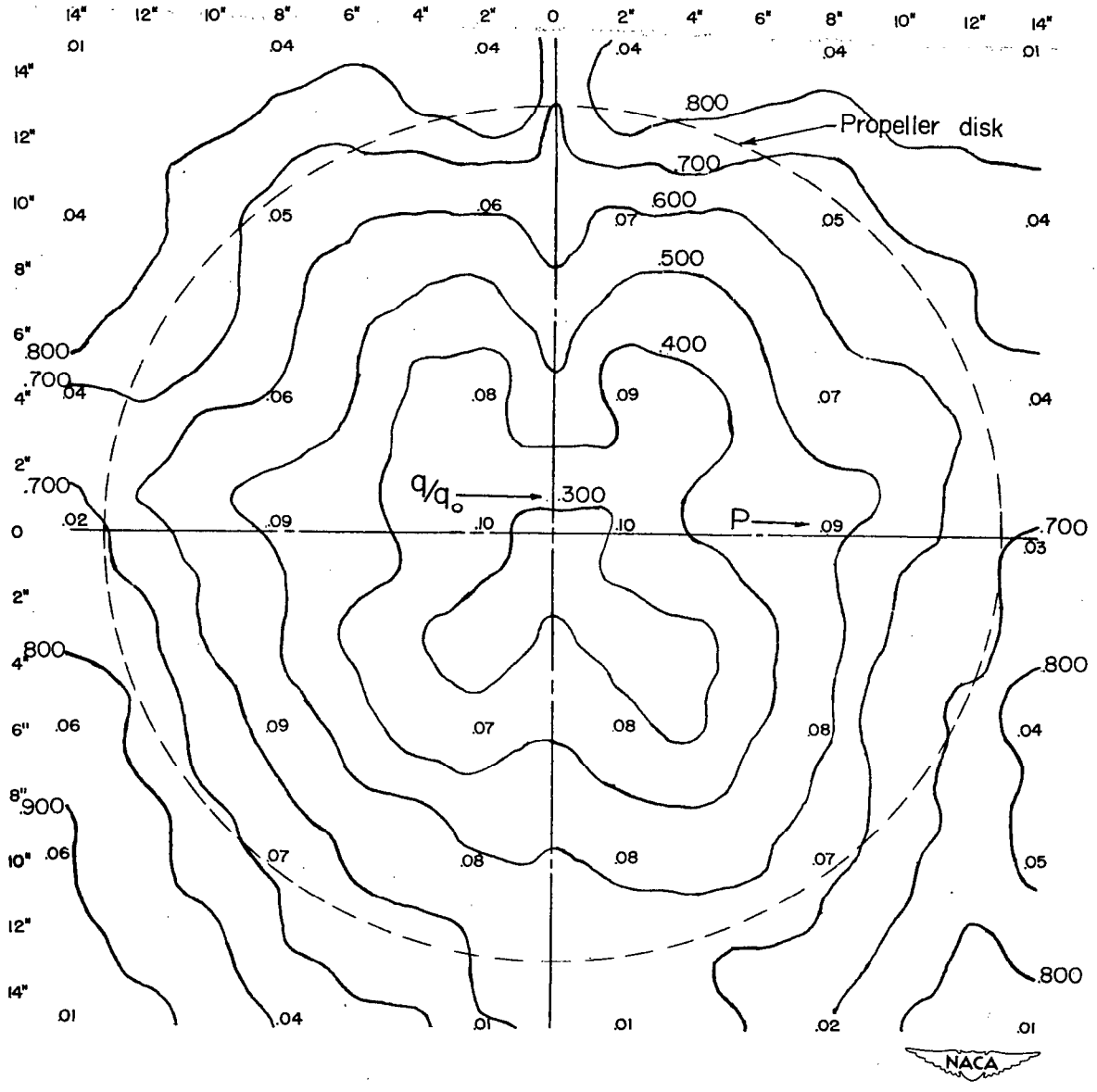

(b) Nine inches aft of propeller.

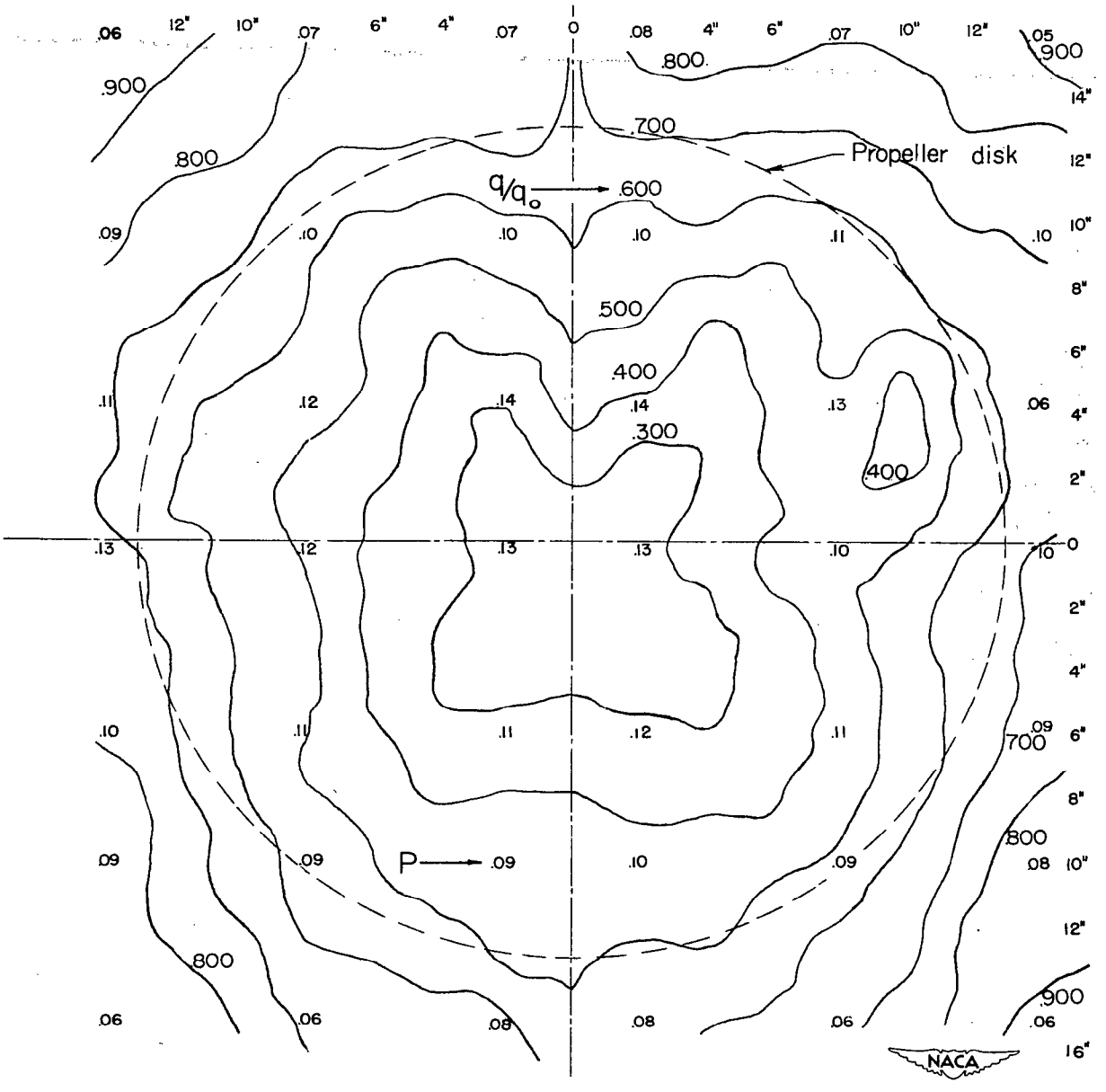
Propeller disk
q/q₀
P
.900
.800
.700
.600
.500
.400
.300
NACA